2004-09

Simulating radiation-induced defects on semiconductor devices

Gladney, Dewey Clinton.

Monterey California. Naval Postgraduate School

NAVAL POSTGRADUATE SCHOOL

MONTEREY, CALIFORNIA

THESIS

SIMULATING RADIATION-INDUCED DEFECTS ON SEMICONDUCTOR DEVICES

by

Dewey Clinton Gladney

September 2004

Thesis Advisor:	Sherif Michael
Second Reader:	Todd R. Weatherford

Approved for public release; distribution is unlimited

THIS PAGE INTENTIONALLY LEFT BLANK

REPORT DOCUMENTATION PAGE			Form Approved OMB No. 0704-0188
Public reporting burden for this collection of information is estimated to average 1 hour per response, including the time for reviewing instruction, searching existing data sources, gathering and maintaining the data needed, and completing and reviewing the collection of information. Send comments regarding this burden estimate or any other aspect of this collection of information, including suggestions for reducing this burden, to Washington headquarters Services, Directorate for Information Operations and Reports, 1215 Jefferson Davis Highway, Suite 1204, Arlington, VA 22202-4302, and to the Office of Management and Budget, Paperwork Reduction Project (0704-0188) Washington DC 20503.			
1. AGENCY USE ONLY *(Leave blank)*	**2. REPORT DATE** September 2004	**3. REPORT TYPE AND DATES COVERED** Master's Thesis	
4. TITLE AND SUBTITLE: Simulating Radiation-Induced Defects on Semiconductor Devices			**5. FUNDING NUMBERS**
6. AUTHOR(S) Dewey Clinton Gladney			
7. PERFORMING ORGANIZATION NAME(S) AND ADDRESS(ES) Naval Postgraduate School Monterey, CA 93943-5000			**8. PERFORMING ORGANIZATION REPORT NUMBER**
9. SPONSORING /MONITORING AGENCY NAME(S) AND ADDRESS(ES)			**10. SPONSORING/MONITORING AGENCY REPORT NUMBER**
11. SUPPLEMENTARY NOTES The views expressed in this thesis are those of the author and do not reflect the official policy or position of the Department of Defense or the U.S. Government.			
12a. DISTRIBUTION / AVAILABILITY STATEMENT Approved for public release; distribution is unlimited			**12b. DISTRIBUTION CODE**

13. ABSTRACT (maximum 200 words)

Exploring semiconductor lifetime, reliability and performance is a never-ending science for today's modern electronics. One significant problem that affects all of these areas is radiation-induced damage. Making calculations to determine how semiconductor devices will hold up in radiation-harsh environments has to be achieved in order to determine system lifetime once placed in their operational capacity. Today's high-technology investments in such areas as satellite design, medical advances, military and commercial hardware, demand thorough understanding in radiation damage. Modeling semiconductor devices with computer-based simulation will provide a cost and time savings over a repetitive design and testing sequence.

This thesis models and simulates an industry standard solar cell and a light emitting diode (LED), using the SILVACO ATLAS$_{TM}$ computer-based program. Using this software, these simulations are generated based on known radiation-induced defects on gallium arsenide (GaAs) semiconductive devices derived from Deep Level Transient Spectroscopy (DLTS) studies. A comparison is then made with another radiation-induced damage prediction method, known as Non-Ionizing Energy Loss (NIEL), to see if the SILVACO ATLAS$_{TM}$ models can be used as an alternative.

14. SUBJECT TERMS Radiation, GaAs Solar Cells, GaAs Semiconductors, Semiconductors			**15. NUMBER OF PAGES** 79
			16. PRICE CODE
17. SECURITY CLASSIFICATION OF REPORT Unclassified	**18. SECURITY CLASSIFICATION OF THIS PAGE** Unclassified	**19. SECURITY CLASSIFICATION OF ABSTRACT** Unclassified	**20. LIMITATION OF ABSTRACT** UL

NSN 7540-01-280-5500 Standard Form 298 (Rev. 2-89)
Prescribed by ANSI Std. 239-18

THIS PAGE INTENTIONALLY LEFT BLANK

Approved for public release; distribution is unlimited

SIMULATING RADIATION-INDUCED DEFECTS ON SEMICONDUCTOR DEVICES

Dewey Clinton Gladney
Lieutenant, United States Navy
B.S., Southern University and A&M College, 1997

Submitted in partial fulfillment of the
requirements for the degree of

MASTER OF SCIENCE IN ELECTRICAL ENGINEERING

from the

NAVAL POSTGRADUATE SCHOOL
September 2004

Author: Dewey Clinton Gladney

Approved by: Sherif Michael
Thesis Advisor

Todd R. Weatherford
Second Reader

John P. Powers
Chairman, Department of Electrical and Computer Engineering

THIS PAGE INTENTIONALLY LEFT BLANK

ABSTRACT

Exploring semiconductor lifetime, reliability and performance is a never-ending science for today's modern electronics. One significant problem that affects all of these areas is radiation-induced damage. Making calculations to determine how semiconductor devices will hold up in radiation-harsh environments has to be achieved in order to determine system lifetime once placed in their operational capacity. Today's high-technology investments in such areas as satellite design, medical advances, military and commercial hardware, demand thorough understanding in radiation damage. Modeling semiconductor devices with computer-based simulation will provide a cost and time savings over a repetitive design and testing sequence.

This thesis models and simulates an industry standard solar cell and a light emitting diode (LED), using the SILVACO ATLAS$_{TM}$ computer-based program. Using this software, these simulations are generated based on known radiation-induced defects on gallium arsenide (GaAs) semiconductive devices derived from Deep Level Transient Spectroscopy (DLTS) studies. A comparison is then made with another radiation-induced damage prediction method, known as Non-Ionizing Energy Loss (NIEL), to see if the SILVACO ATLAS$_{TM}$ models can be used as an alternative.

THIS PAGE INTENTIONALLY LEFT BLANK

TABLE OF CONTENTS

LIST OF FIGURES

THIS PAGE INTENTIONALLY LEFT BLANK

LIST OF TABLES

THIS PAGE INTENTIONALLY LEFT BLANK

ACKNOWLEDGMENTS

The author would like to thank the following individuals: his parents, Mr. and Mrs. Dewey and Josephine Gladney, for their steadfast support during his tour at NPS and throughout his military career; Professor Sherif Michael for his inspiring confidence, advice and guidance; Professor Todd R. Weatherford for his exceptional direction, time and support; Nancy Sharrock for her assistance with this thesis and being a superb friend; and the entire Naval Postgraduate School faculty and staff for providing a fine graduate education.

THIS PAGE INTENTIONALLY LEFT BLANK

EXECUTIVE SUMMARY

Exploring semiconductor lifetime, reliability and performance is a never-ending science for today's modern electronics. One significant problem that affects all of these areas is radiation-induced damage. Making predictions to determine how semiconductor devices will hold up in radiation-harsh environments has to be achieved in order to determine how long they will last once placed in their operational environment. Today's high technology investments in such areas as satellite design, medical advances, military and commercial hardware, demand thorough understanding of radiation damage.

In many studies, Non-Ionizing Energy Loss (NIEL) has been used to estimate a degradation factor relating to radiation fluence [Ref. 1]. In this thesis, this method will be examined and compared to radiation predictions developed by utilizing the commercially available SILVACO ATLAS$_{TM}$ Virtual Wafer Fabrication program. Using this program, models of a light emitting diode (LED) and a solar cell were created to examine how well the computer-based program's radiation predictions compared to the NIEL radiation predictions.

The first challenge of this thesis was to model the solar cell and the light emitting diode, utilizing the SILVACO ATLAS$_{TM}$ program. These simulations were generated based on known radiation-induced defects on gallium arsenide (GaAs) semiconductive devices derived from Deep Level Transient Spectroscopy (DLTS) studies. A comparative analysis was then conducted between the NIEL predictions and the SILVACO ATLAS$_{TM}$ program predictions to establish the validity of using computer-based software as an alternative radiation prediction method.

The primary objective of this thesis was to validate the utilization of the SILVACO ATLAS$_{TM}$ Virtual Wafer Fabrication program for the prediction of radiation-induced defects in semiconductor materials. This was achieved by introducing defects into the constructed models using a trap statement that activates bulk traps at discrete energy levels within the bandgap of the semiconductor material. In addition to having the capability to modify doping profiles in semiconductive materials, the SILVACO

ATLAS$_{TM}$ program also allows the user to change the energy level of defects, the depth of traps, the density of traps, the charge type of traps and the size of traps. These unique capabilities give the SILVACO ATLAS$_{TM}$ program the ability to simulate radiation-induced defects with reliable and consistent results. The overall accuracy of this prediction method is ultimately limited by the accuracy of the SILVACO ATLAS$_{TM}$ program parameter-defects that were implemented into the simulation codes.

I. INTRODUCTION

A. BACKGROUND

Why study radiation-induced defect prediction methods of semiconductor devices?

Today's military electronic devices operating in radiation harsh environments sustain radiation-induced damage that has a direct effect on system lifetime. Some of these defects affect the semiconductor lattice (e.g., the position of atoms within the material) structure and therefore may alter device performance. For example, in space and near-space altitudes, solar cells used on satellites for power generation degrade as a result of permanent damage introduced to the semiconductor material lattice from extended exposure to radiation. The rate of degradation can be closely predicted and satellite designers rely on this prediction to determine their spacecraft's lifetime once placed in its operational environment.

In this thesis, radiation-induced defects on a GaAs light emitting diode and solar cell are simulated using the SILVACO ATLAS$_{TM}$ computer-based program. For the light emitting diode, changes to defect density are shown to affect its luminescent intensity; similarly for the solar cell, these changes are shown to affect its *I-V* characteristics.

As will be discussed later, by implementing parameters into the SILVACO ATLAS$_{TM}$ program, radiation defects are modeled based on experimental data derived from known irradiated material [Refs. 2, 3]. Once matured, benefits attained through modeling radiation damage in computer-based programs vice actually growing, testing and irradiating semiconductor materials will significantly enhance semiconductor testing and reliability.

B. PURPOSE

The purpose of this research was to model a light emitting diode and a solar cell; introducing radiation-induced defects within SILVACO ATLAS$_{TM}$ models to examine how luminescent light intensity for a light emitting diode and *I-V* characteristics for a so-

lar cell change as different defects are simulated. The results were then compared to another radiation-induced damage prediction method, NIEL, to verify whether or not the SILVACO ATLAS$_{TM}$ models can be used as a valid alternative.

C. THESIS OVERVIEW

Understanding the nature of radiation-induced defects before the production of a semiconductive device can significantly reduce many of the risk factors associated with the extensive qualification and system fielding processes. This thesis demonstrates that having the ability to predict semiconductor degradation resulting from radiation-induced damage using a computer-based program could be a valid method for future radiation damage predictions.

Chapter II gives background information describing semiconductor basics so that a novice reader may understand how radiation affects semiconductive material. Chapter III describes radiation fundamentals and how they relate to a solar cell and a light emitting diode. Chapter IV gives general subject matter information regarding radiation-induced effects on semiconductive devices. Chapter V explores the use of SILVACO ATLAS$_{TM}$ as a semiconductor simulation tool used in radiation-induced damage predictions. In Chapter VI, results of the radiation-induced defects implemented into the SILVACO ATLAS$_{TM}$ models are examined to analyze how their output characteristics compared to NIEL and other radiation prediction methods. Finally, Chapter VII concludes this thesis and provides several recommendations for future analysis.

II. BACKGROUND

A. CHAPTER INTRODUCTION

The initial step towards beginning to understanding how radiation affects semiconductive devices is to first understand device operation. This chapter discusses basic operations of semiconductor devices.

B. BASIC SEMICONDUCTOR PHYSICS

1. Energy Bands

Semiconductors are the fundamental basis for modern electronics because they control conductivity using applied energy. They possess the unique ability to behave as conductors as well as insulators. Thus, semiconductors are of little value unless constructed so they can perform these characteristics with proven reliability and sustained stability.

The semiconductor relationship to familiar materials such as conductors and insulators can help explain this concept. An illustration of these devices and their relationships is given below in Figure 2.1.

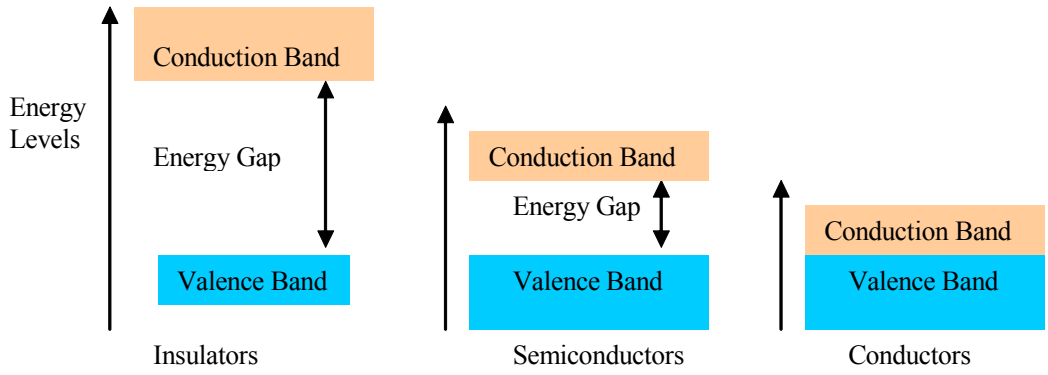

Figure 2.1. Semiconductor Energy Band Diagram

In insulators, the electrons in the valence band are separated by a large gap (e.g., the energy gap) from the conduction band as illustrated by the left-most device in Figure 2.1. In the illustration of conductors, right-most device in Figure 2.1, the valence band is seen to overlap the conduction band leaving essentially no energy gap. In the illustration

of semiconductors, a small gap does exist between the valence and conduction bands in which thermal, applied voltages or other excitations can cause electrons to migrate from the valence band to the conduction band.

Figure 2.1 relates the bandgap variances between insulators, semiconductors and conductors; and, as this visual representation illustrates, the larger the bandgap, the more energy is required to migrate electrons from the valence band to the conduction band. In short, the larger this energy gap, the more energy required to begin the conduction of electrical current. Manipulating these materials by introducing various impurities (e.g., doping) can increase or reduce their conductivity controlling characteristics.

In the semiconductive material, electrons are forced into specific energy levels called allowed states**.** They are then grouped into specific configurations called energy bands. One is the conduction band and the other is the valence band. The forbidden gap is between these energy bands and is commonly called the bandgap. The conduction band is typically free of electrons and the valence band is typically a full band of electrons. When electrons begin to move to other locations in the bands, wherever they have moved from thus becomes a more positive state. In the valence band, this vacant state is now called a hole. This apparent migration can be thought of as holes and electrons moving. These free electrons and holes are called the charge carriers. The carrier with the greater concentration is called the majority carrier while the carrier with the lesser concentration is called the minority carrier. These processes in which electron-hole pairs are created is called generation. The process by which electrons return to the valence band, thus annihilating electron-hole pairs, is called recombination [Ref. 3].

2. Solar Cell and Light Emitting Diode (LED) Basics

Modern electronics greatly involves optical and electrical processes. In many cases they work together, hand-in-hand. Solar cells and light emitting diodes are both part of the optoelectronic family of semiconductor electronic devices. Optoelectronics involves the interaction of light photons with semiconductors and are used in a variety of applications. They often provide the optical sources and detectors that allow broadband telecommunication via fiber-optic networks spanning thousands of global miles.

a. The Solar Cell

Devices that convert optical energy (e.g., notably sunlight) into electrical energy are typically known as solar cells. When light strikes the cell, a certain portion of its energy is absorbed and transferred into the semiconductor material. This energy elevates electrons above their original valence shells in the conduction band. Depending on device construction, positive or negative electric fields of the pn-junction (e.g., *p*-type region for positive, *n*-type region for negative) within the semiconductor material force the electrons to flow in a certain direction. This flow of electrons is photo-current. This current can be extracted and used externally by placing metal contacts on the top and bottom of the semiconductor material. The measured current and voltage generated typically defines the power the solar cell can produce.

For space applications, radiation that exists outside the earth's atmosphere significantly affects the solar cell's power generating lifetime. High-energy particles enter the cell and create imperfections in the lattice structure that act as recombination or trapping centers. Particle bombardment is continuous in space; thus the solar cell's output power gradually decreases with elapsed time [Refs. 3, 4].

b. The Light Emitting Diode (LED)

Emitters of photons by applied current include light emitting diodes. Photons consist of small particle-like packets that have energy and momentum but no mass. Generally, a light emitting diode consists of a p-type region and n-type region to form a pn-junction. When sufficient voltage is applied across the leads of the light emitting diode, electrons in the n-type region of the material gain sufficient energy to move across the junction into the p-type region. Once in the p-type region, the electrons are immediately attracted to the positive charges due to the mutual forces of attraction between opposite electric charges. When these electrons move close to the positive charges in the p-type region, the two charges recombine. Each time this recombination occurs, a photon of luminous energy equal to the material's bandgap energy is released [Refs. 3, 5, 6].

C. THE DARK CURRENT

Photodiodes produce another current even when no light is incident on them in addition to photocurrent. This current is referred to as the dark current and is the primary source of the thermal excitation of electrons in photodiodes at room temperature. The dark current acts as a source of background noise that is the unwanted current that sometimes masks the wanted photocurrent of faint optical signals [Ref. 7].

D. CHAPTER SUMMARY

This chapter described basic semiconductor physics for a solar cell and light emitting diode. This general understanding is necessary to explain how radiation affects their operation in radiation harsh-environments. The next chapter discusses background information regarding radiation and the effects of that radiation on semiconductors.

III. RADIATION FUNDAMENTALS

A. CHAPTER INTRODUCTION

The earth's radiation environment includes photons, electrons, protons and heavy ions. They are usually divided into two categories, trapped and transient. The earth's core is mostly iron which creates a magnetic field around the earth trapping both electrons and protons in what are referred to as Van Allen Belts. Surrounding the earth exist a proton belt that has a dip near the southeast coast of South America. This commonly is referred to as the South Atlantic Anomaly (SAA). The SAA is the source of most of the harmful radiation for space systems operating in the Low Earth Orbit (LEO). The energy of the protons in the proton belt is higher nearer the earth and can reach 400 million electron volts (MeV) [Refs. 4, 8, 9].

B. RADIATION ENERGY TERMS

To understand the complex list of radiation levels and exposure rates, the following terms are defined as follows [Ref. 5]:

eV	A unit of energy equivalent to $1.6\times10^{-19}\,\mathrm{J}$.
keV	10^3 eV
MeV	10^6 electron volts
GeV	10^9 electron volts
Dose rate	The rate energy is delivered or absorbed.
Flux	Flux defines the number of particles, photons or energy passing through a given area in a specified time. Flux may also be specified in terms of the number of particles per unit time passing through an area on the surface of a sphere enclosed by a solid angle.
Fluence	Particle fluence is defined as the number of particles traversing a unit area in a unit period of time.

C. UNDERSTANDING TRAPS

High levels of unshielded radiation particles can cause defects in virtually all semiconductive devices. Some of these defects introduce trapping energy states, which correspond to physical recombination sites created within the material's lattice (see Figure 3.1 below). The trapping energy states are usually at shallow energy levels just inside the forbidden gap near the conduction band edge for donor-type traps and just inside the forbidden energy gap near the valence band edge for acceptor-type traps. The different types of defect clusters are known to correspond to different kinds of donor and acceptor traps. The resulting effect is that these traps reduce minority carrier lifetimes, τ . The degradation of the minority carrier lifetime resulting from the introduction of traps within the bandgap is defined as

$$1/\tau = 1/\tau_i + \Phi_n / K \tag{3.1}$$

where τ_i is the unirradiated value of the minority carrier lifetime, Φ_n is the incident neutron fluence, and K is the damage constant. Equation 3.1 assumes fluence is proportional to minority carrier lifetime [Ref. 12]. (In this thesis, Equation 3.1 is not used to estimate minority carrier lifetime; the SILVACO ATLAS$_{TM}$ program derives this from given parameters.)

As seen in Figure 3.1 below, traps are typically generated between the valence band and the conduction band but remain close to the band's edge, just inside the forbidden energy gaps.

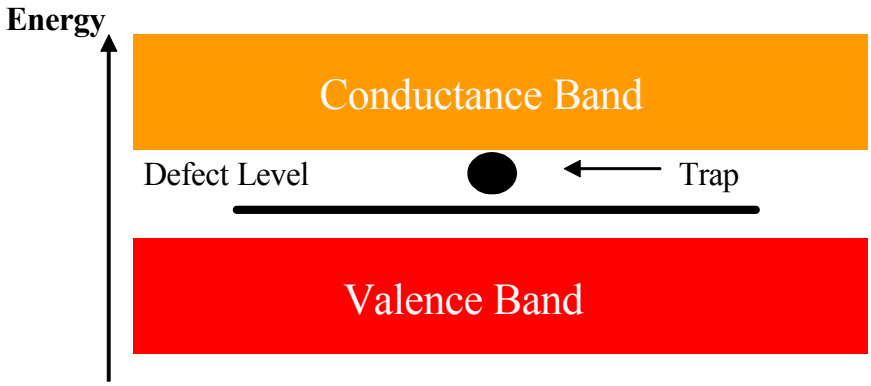

Figure 3.1. Carrier Trap Location

Using the SILVACO ATLAS$_{TM}$ program, some of the parameters seen in Figure 3.1 such as the defect level, trap depth, trap density, trap charge type and trap size can be implemented into the simulation programs.

D. RADIATION RELATIONSHIPS

Comprehension of some basic radiation relationships is required in order to understand the damage caused in the semiconductive devices.

1. Radiation Types

There are several types of radiation [Ref. 5]:

- Beta particles are identical to electrons. They carry one negative electron charge.
- Alpha particles are heavier. They are identical to the nucleus of a helium atom, with two protons and two neutrons, and have a positive electrical charge of $+2$.
- Positrons are equal in mass to electrons and have an equal but opposite positive electrical charge.
- Neutrons are approximately equal in mass to the proton and have no electric charge.

E. RADIATION AND RADIATION-INDUCED DAMAGE

It is first necessary to understand what radiation and radiation-induced damage are before exploring the problems that radiation may cause in today's electronics.

Radiation is the propagation of energy in the form of waves and/or particles that may vary in frequency as well as wavelength. It is also possible to describe this propagation of energy according to its position on the electromagnetic spectrum. Radiation includes but is not limited to X-rays, gamma rays, ultraviolet light, visible light, infrared light and radio waves.

According to the quantum theory model, electromagnetic radiation consists of bundles of energy called photons that travel at the speed of light. Gamma rays and X-rays are both photons but differ in origin. Gamma rays result from transformations that take place in the nucleus of an atom, whereas interactions outside the nucleus form X-rays [Refs. 3, 10].

In general, all semiconductors devices are susceptible to radiation damage. Radiation damage in optoelectronics occurs primarily through the creation of deep traps within the energy bandgap that reduces the minority carrier lifetimes. The radiation type usually of interest in the study of the degradation to electronic devices consists of energetic or fast, massive particles (e.g., electrons, protons, neutrons or ions). The origin of these particles may be particle accelerators, the natural space radiation environment or nuclear reactions. Since they have mass, energy and possibly charge, these particle or other particles generated by them, can interact in a variety of ways with semiconductive materials [Ref. 3].

F. RADIATION EFFECTS

The study of radiation effects on electronics can be divided into several categories according to their effect to the electronic device. This thesis simulates displacement and proton radiation-induced damage within the semiconductor models and discusses their effects.

1. Displacement Damage

The effect of displacement damage in semiconductors depends on several factors including but not limited to wavelength, doping levels and physical make-up (e.g., device construction). Displacement damage reduces minority carrier lifetime, which affects diffusion length. This relationship can be defined as

$$L = \sqrt{D\tau} \tag{3.2}$$

where L is the diffusion length, D is the diffusion constant and τ is the minority lifetime. Semiconductors with shorter penetration depths to the active regions have increased sensitivity to displacement damage because the radiation is absorbed in the upper regions.

Semiconductor devices rely on the crystalline structure of the semiconductor material for their operation. When high-energy particles penetrate the semiconductor, inelastic or elastic reactions may occur with the semiconductor atoms, resulting in their displacement from their original crystalline position. This is known as displacement damage and can be characterized by the radiation prediction method known as Non-Ionizing Energy Loss (NIEL). In short, NIEL is the energy a particle imparts to a solid through

mechanisms other than ionization and has been characterized for many particles as a function of particle energy. Displacement damage is often characterized by the NIEL of the incident particles as they pass through the semiconductor. The damage factor, which is a measure of the degradation to an electronic device resulting from displacement damage, is normally proportional to the fluence of particles. The primary particles that cause displacement damage in the space environment are protons. Although heavy ions typically have a much higher NIEL, they are not as abundant [Ref. 8]. (Further discussion of NIEL is offered in the results section of this thesis, Chapter VI.)

Displacement damage causes degradation to several semiconductor properties which may lead to gradual system failure. The most severe problem is the generation of recombination centers that reduce minority carrier lifetime; leading to gain degradation in bipolar devices, less power efficiency in solar cells and degraded luminescent intensity in light emitting diodes. Since MOSFETs and JFETs are majority carrier devices rather than minority carrier devices, they do not suffer from this effect significantly [Ref. 8].

a. Damage Range

High-energy proton and electron radiation cause most of the permanent damage in semiconductors and semiconductor alloys in, for example, the space environment. Low MeV energy protons, and especially alpha particles, may be shielded significantly by the material composing the spacecraft's skin and, additionally, by the material surrounding the device itself. In contrast, high MeV energy protons may pass through most of this shielding and damage the device. Thus, for a study of displacement damage in a device for space applications, it is essential to study radiation damage over a wide range of energy, 1 to 500 MeV [Ref. 5].

2. Proton Radiation Damage

A proton has a positive electrical charge, equal and opposite to that of the electron. If isolated, a single proton would have a mass of only 1.673×10^{-27} kg. Using GaAs as an example, protons can cause two kinds of damage:

- Displacement damage where atoms are knocked off their sites to become traps.
- The creation of irregular electron-hole pair formations.

The use of NIEL for determining proton damage in semiconductors has been utilized extensively over the years as a method of radiation-induced damage prediction. The comparison of this prediction method to SILVACO ATLAS$_{TM}$ predictions is one of the objectives of this thesis [Refs. 3, 9, 10].

G. RADIATION HARDNESS

Radiation hardness for displacement defects is determined in part by the displacement threshold energy, E_d, which is defined as the minimum energy required to transfer a lattice atom from its equilibrium position to an interstitial one. The larger the E_d, the more resistant the material is to radiation. For GaAs, E_d is 9.8 eV [Ref. 13]. Ensuring the reliable operation of electronics in a radiation-harsh environment is a complicated and expensive task. The radiation hardness qualification process is made more difficult by limited access to radiation testing facilities and the variety of the radiation hardness levels in commercial components. Radiation hardness qualifications typically consists of the following tests [Refs. 3, 14]:

- Total dose using an X-ray tests on unpackaged chips.
- Displacement damage using neutrons from a nuclear reactor or special neutron sources.
- Single event tests using high-energy proton beams (e.g., 60 MeV and above).

As an objective of this thesis, having the ability to model semiconductive devices in a computer-based program to examine changes to its electronic characteristics once exposed to harmful radiation levels will greatly reduce the time and cost associated with these qualification processes.

1. Radiation Hardness Applications

a. Commercial Off the Shelf (COTS)

For COTS electronic components, the radiation qualification is often seriously compromised because components with the same component identification may potentially come from alternative fabrication lines with significantly different radiation hardness characteristics. These products often do not qualify for military applications.

b. Radiation Hardness of III-V Compound Semiconductor Alloys

Semiconductor alloys manufactured from III-V compounds, such as GaAs, often exhibit good characteristics for radiation hardness. The relatively large absorption coefficients of III-V compounds allow the manufacture of very efficient semiconductor alloys with thin active regions; because for a given fluence, a small active region has fewer radiation-induced defects than a large active region. Therefore, a thin action region causes III-V compounds to have less displacement damage than other semiconductor alloys. Additionally, III-V compound photodiodes exhibit less susceptibility to ionizing radiation than other semiconductor alloys. The internal electric fields associated with the heterostructure configurations used in the fabrication of semiconductor alloys from III-V compounds inhibit the movement of the excess carriers generated by ionizing radiation [Refs. 6, 7].

H. CHAPTER SUMMARY

This chapter described basic radiation fundamentals and how they relate to solar cells and light emitting diodes. The next chapter describes the various radiation-induced defects caused in semiconductor devices.

THIS PAGE INTENTIONALLY LEFT BLANK

IV. RADIATION EFFECTS

A. CHAPTER INTRODUCTION

Radiation fundamentals discussed in the previous chapter will be utilized in this chapter to examine the effects of radiation on semiconductor operation. This chapter also examines the process ultimately used to overcome some of the difficulties encountered while simulating radiation defects.

B. CELL DEGRADATION DUE TO RADIATION

1. Parameters

Before examining how the simulations were developed, it is important to understand the radiation parameters used within the SILVACO ATLAS$_{TM}$ models. To help evaluate these parameters, the following information is provided regarding cell degradation caused by radiation-induced defects:

- The concentration, N_C, of the compensating centers (e.g., number of defects, which compensate the doping concentration).
- The concentration, N_R, of the recombination centers (e.g., number of defects, which induce minority carrier recombination).
- The associated electron and hole capture cross-sections (e.g., σ_n and σ_p) of the recombination centers.
- The capture cross-section relationship to the other parameters:

$$\tau_{n,p} = \frac{1}{N_R v_{n,p} \sigma_{n,p}} \tag{4.1}$$

where $v_{n,p}$ is the thermal velocity of the carriers. The minority carrier lifetime, τ, can be calculated directly from τ_n and τ_p. Lifetime measurements provide the product $N_R v_{n,p}$ [Ref. 11].

When radiation-induced defects begin to affect semiconductor characteristics, a variety of defects may occur within its bandgap. Figure 4.1 illustrates some of the known defects that take place in semiconductors that may affect their intended operation.

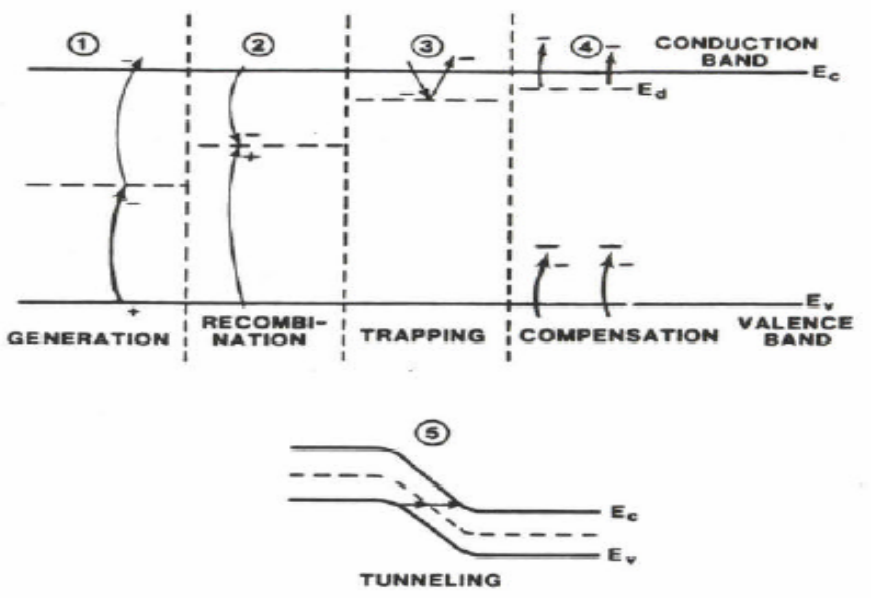

Figure 4.1. Five Effects That Can Occur Due to the Presence of Defects in Semiconductor Bandgaps [From Ref. 8.]

With no applied energy, at equilibrium, atoms inside semiconductors are not at rest. An excess or deficit in the carrier concentrations relative to their equilibrium value are created within the semiconductive material. Electron-hole pairs continue to be created and eliminated yet the overall net effect remains zero. This process of creation and elimination is called *recombination* and *generation*, respectively. *Generation* creates electron-hole pairs whereas *recombination* removes electron-hole pairs. It is nature's order-restoring mechanism, whereby the carrier excess or deficit inside the semiconductor is stabilized or eliminated. Since non-equilibrium conditions are continuous during device operation, these processes are typical in semiconductors functioning properly. However, when exposed to harmful radiation dosages these processes can be induced, resulting in a disruption of intended device operation. In this regard, *recombination* and *generation* are justly defined as radiation-induced defects.

Other defects known to be caused by harmful radiation exposures are *traps, compensation* and *tunneling*. *Traps*, as mentioned previously, hold electrons in the energy gap resulting in a decrease in the semiconductor's carrier lifetime. C*ompensation* allows too many electrons to enter the energy gap causing a decrease in the stability of semiconductive devices. Compensation capacitors are sometimes incorporated into system design

to counter the effects of this defect as they gradually become more apparent over time. Finally, the most uncommon defect discussed here is *tunneling*; which allows electrons to jump across the energy gap without changing their energy level. This defect can result in device instability and sometimes leads to inadequately-responsive device operation [Refs. 3, 4].

This thesis only examines the effects *traps* have on semiconductive devices and does not attempt to simulate any of the other mentioned defects.

C. MEASURING RADIATION DEFECTS

1. Deep Level Transient Spectroscopy (DLTS)

The concentrations of defects can be measured using transient capacitance techniques called DLTS [Ref. 1]. DLTS is a form of signal processing that displays the temperature-dependent emission transients; producing a sequence of peaks, each of which could be interpreted relating to an electrically active defect. This process has become very popular for studying deep defect levels in semiconductor materials.

2. Velocity Versus Size

If a subject ion enters a crystal lattice structure at a very high velocity, little time exists for the ion to transfer any energy to the lattice atoms. This is similar to a fast bullet leaving a small hole in a target, unlike a slow shotgun slug leaving a large hole in the same target. In short, the maximum Linear Energy Transfer (LET) occurs where the subject ion is most efficient in transferring energy to the crystal [Ref. 10]. This maximum energy point is typically towards the end of the ion's impact range within the semiconductor. The Rutherford scattering radius, r_d , calculates the cross-section for an interaction [Ref. 13]. The relationship is given as

$$r_d = \frac{kq_\alpha Q}{\frac{m_\alpha v^2}{2}} \tag{4.2}$$

where q_∞, m_α and v are the charge, mass and velocity of the subject particle, respectively; Q is the atomic charge of the target; and k is the coulomb constant. The bottom term is the kinetic energy of the particle. Thus higher energy particles have lower cross-sections for scattering.

These coulombic forces are not the only elements acting on semiconductors as a result of radiation. Nuclear effects can also occur for much smaller cross-sections. The nuclear interaction can be either [Ref. 5]:

- elastic – where the nuclear forces repel the lattice atom from the subject heavy ion.
- inelastic – where the two atoms' nuclei are absorbed and new particles are released.

In either case, a lattice atom was moved or a new moving ion was created.

D. PHOTOGENERATION AND POWER

When external thermal energy is absorbed in a solar cell and its energy is then transferred into the semiconductive material, photogeneration is said to occur. Light photons with sufficient energy interact with the semiconductive atoms creating electron-hole pairs. As different amounts of photons bombard the material, this electron-hole pair creation rate changes. These changes in rates and in wavelength also correspond to changes in the electrical output of the device. The wavelength, λ, of a photon is inversely proportional to the energy it creates, E. This relationship is given as

$$E = \frac{hc}{\lambda} \tag{4.3}$$

where h is Planck's constant (4.136×10^{-15} eV-s) and c is the speed of light.

A discussion of photogeneration and power must also include their energy source. With this said, examination of these solar cell properties should logically begin with the understanding of the sun's energy. The amount of photons and their respective energy levels can be determined by examining the solar spectrum of the sun. This spectrum is comprised of metrics that measure the level of the energy radiating throughout the earth's environment. Air Mass Zero (AM0) corresponds to the average light spectrum seen just

outside the earth's atmosphere where no conditions exist to attenuate its intensity; it has a spectral power density of approximately 135.3 mW/cm^2. AM1 corresponds to the solar intensity at the point where the incident light is normal to the earth's surface. Most terrestrial solar research assumes an air mass of AM1.5 and is representative of the average solar intensity measured at sea level during daylight. AM1.5 is normalized to yield a spectral power density of approximately 100 mW/cm^2 [Ref. 13].

As discussed previously, dark current is produced in solar cells even when no light is incident on them. Dark current flows in the opposite direction of the conducting current in an active solar cell and therefore degrades device performance over time. To accurately determine the *I-V* characteristics of a solar cell, the photogenerated current minus the dark current must be taken into account. This relationship is given as

$$I = I_L - I_D \tag{4.4}$$

where I_L is defined as the current produced when photogeneration is taking place and I_D is defined as the current produced when photogeneration is not taking place (i.e., the dark current). Figure 4.2 graphically demonstrates this relationship.

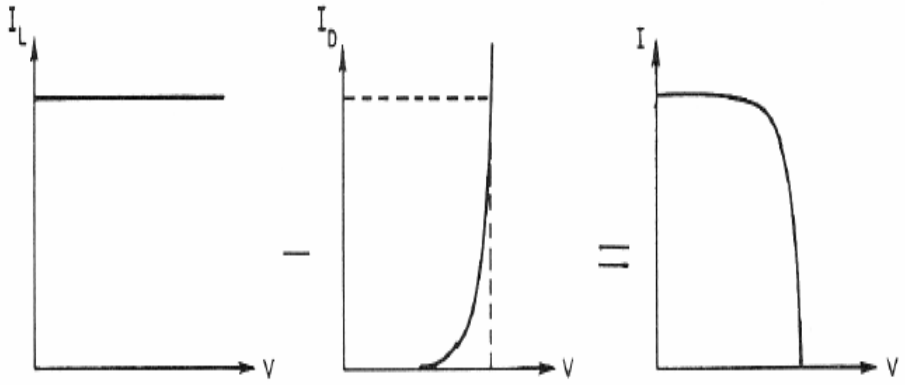

Figure 4.2. Graphical Representation of Solar Cell Current [From Ref. 16.]

A solar cell's *I-V* characteristics is determined by measuring the voltage and current produced when light photons are exposed to its collective surface. The maximum power of the solar cell is given as the maximum current and voltage product of the cell's

I-V curve. Each constructed solar cell has its own unique *I-V* curve and can be displayed graphically by extracting measurements from its produced current and voltage at particular instances in time. The graphical illustration farthest right in Figure 4.2 is the net result of the light and dark currents and is typically shown as a standard solar cell's *I-V* curve. The shape of the knee-like bend is an important trait to observe. Solar cells designed for optimum performance are seen to have sharper bends, whereas poorly designed, less efficient cells typically have more curved bends.

Later in the results section of this thesis, Chapter VI, the shape of the constructed solar cell's *I-V* will be examined as well as its follow-on subsequent *I-V* curves. These curves will be seen to undergo slight changes in curvature resulting from the defects that were introduced into its SILVACO ATLAS$_{TM}$ model.

Another very important characteristic of solar cells is the efficiency at which it converts the maximum amount of available solar energy into useful electrical energy. The higher the efficiency, the lower the cost and receptive collection area required to achieve the desired electrical output. In the right side of Figure 4.2, the maximum current at $V = 0$ is called the short circuit current, I_{SC}. The maximum voltage at $I = 0$ is called the open circuit voltage, V_{OC}. Figure 4.3 below offers a more descriptive view of the *I-V* curve for a solar cell, illustrating its maximum output power.

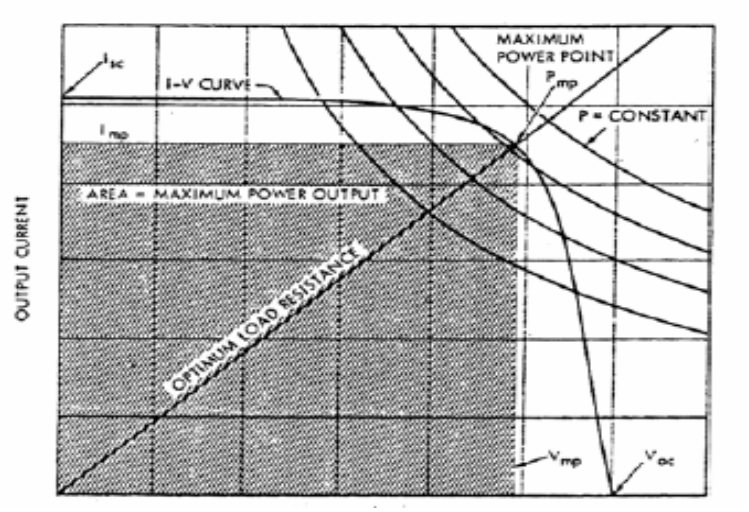

Figure 4.3. Maximum Power Rectangle for a Solar Cell [From Ref. 16.]

The maximum output power of a given solar cell is the maximum area as outlined by the shaded region in Figure 4.3 and is defined by the current and voltage product along its generated *I-V* curve. The associated voltage and current at its maximum output power point, observed at the upper right edge of the shaded region, are labeled V_{mp} and I_{mp}, respectively. These are the operating points of the voltage and current that yields the maximum output power of the solar cell. The open circuit voltage, V_{OC}, is the maximum voltage that can be supplied by the solar cell from a given photo-source and the short circuit current, I_{SC}, is the maximum current that can be extracted from the cell. The term fill-factor, FF, is introduced here with the following relationship

$$FF = \frac{P_{max}}{I_{SC}V_{OC}} = \frac{I_{mp}V_{mp}}{I_{SC}V_{OC}}. \tag{4.5}$$

For assessments of solar cell performance and operation, the term FF was derived to relate the cell's *I-V* characteristics in a single metric.

As discussed earlier, solar cells generate power in proportion to the amount of photon energy incident on its collective surfaces; meaning, the available output power shifts with the available input power. With this being said, it is also known that the solar cell's power efficiency is dependant on the resistance of the load. The power efficiency of the solar cell is defined as the ratio of the maximum power (P_{max}) delivered to the load resistance, to the incident solar power (P_{in}) delivered to its collective surfaces. Along the optimum load resistance line observe in Figure 4.3, the optimum power deliverable to the load is illustrated. The current and voltage seen along this line are the optimal values utilized in calculating the power efficiency of the solar cell. Assuming that the *I-V* curve in Figure 4.3 was taken under AM 0 conditions, the power efficiency, η, of the solar cell can be given by

$$\eta = \frac{P_{max}}{P_{in}} = \frac{I_{mp}V_{mp}}{P_{in}}, \tag{4.6}$$

where P_{in} is the optical input power and is equal to 135.3 mW/cm^2. The power efficiency of a single-crystal silicon solar cell can reach almost 17%, while a single-crystal gallium arsenide cell can reach 20% [Refs. 13, 16].

To further understand causes of poor solar cell power efficiency, the following list taken from previous thesis work is provided [Ref. 16]:

- Reflection of light off the cell surface – If no antireflection coating is applied to the solar cell, part of the light will be reflected off the surface which can sometimes be up to 36%. With antireflection coating and/or a textured surface applied to the receptive surfaces of the solar cell, this degradation can be reduced to 5%.
- Too much or too little energy – Too much energy by a photon that is absorbed by a solar cell can create unwanted electron-hole pairs as well as heat. Particles with too little energy can sometimes not generate wanted electron-hole pairs and only result in an increase in cell temperature.
- Internal recombination – This is unavoidable for cell operation but solar cell layer thickness is kept to an optimum level to insure the carriers have a good probability of reaching the solar cell's power extraction metal contacts.
- Series resistance – This is the natural resistance that exists in the semiconductive material and at the metal contacts that reduce the cell efficiency, generating unnecessary heat and loss in power.
- Material defects – These are impurities within the semiconductive material that cause recombination problems in its bandgap.

E. LIMITATIONS

Available research on semiconductors has shown that radiation-induced damage is stable for long periods of time for devices that are unbiased, but considerable annealing occurs when the devices are biased after or during irradiation due to recombination-enhanced annealing. This can create experimental inconsistencies because less damage occurs in devices operating during irradiation making it difficult to compare biased and unbiased irradiation data results. Uncertainty also exists between experiments conducted for relatively short durations of time with those that were biased longer [Ref. 17].

This thesis only looks at the post-irradiated defects on devices with no respect to time and does not make the distinction of whether or not the device was biased during irradiation.

F. RADIATION DEFECT DATA

1. Defect Data Sources

This thesis compares NIEL radiation-induced damage predictions to those resulting from the SILVACO ATLAS$_{TM}$ simulation models. During research efforts to locate defect data sources, it was discovered that some of the required DLTS data essential for more accurate simulations was not readily available [Refs. 3, 18]. This thesis made use of available DLTS data taken from lab results of high-energy, nitrogen-irradiated Au/n-GaAs Schottky Barrier Diodes taken from Reference 21 to gain equal understanding of the defects introduced in the material by irradiation with protons. The radiation-induced defects that were implemented in the SILVACO ATLAS$_{TM}$ models were based on these samples. With this known, the curves produced should be nevertheless similar for protons because proton radiation damage is closer to nitrogen radiation damage than damage produced by other heavier ions.

As more defect data is made readily available in regard to DLTS studies derived from irradiation damage test results, the SILVACO ATLAS$_{TM}$ simulations will deliver more comprehensive and accurate radiation damage predictions.

2. Group III-V Semiconductor Alloys

A variety of semiconductor materials can potentially be utilized to construct solar cells and light emitting diodes. When the prerequisite is high efficiency, GaAs becomes the material of choice because only some materials can be grown possessing all the traits that include good crystalline quality, controlled impurity content and a long lifetime. GaAs also possesses the overwhelming advantage of being a sufficiently well mastered technology of mass production.

Information derived from defects caused by the irradiation of GaAs semiconductive devices leads to the study of defects in other GaAs alloys, such as GaAlAs or InGaAs. The characteristic of these defects, such as its energy-level and its location in the bandgap, provides important information that can be extended to all of its GaAs semiconductive alloys [Refs. 1, 5].

a. Radiation Hardness of III-V Semiconductor Photodiodes

There are several reasons why photodiodes manufactured from III-V compounds exhibit characteristics of good radiation hardness. For one, III-V compounds have fewer oxides when compared to other semiconductive compounds. Next, the relatively large absorption coefficients of III-V compounds allow the manufacture of very efficient photodiodes with thin active regions. For a given fluence, these thin active regions have fewer radiation-induced defects than a large active region. A thin action region causes III-V compound photodiodes to have less radiation-induced dark currents, for example, than other photodiodes. Additionally, because the direct bandgap III-V compounds have been shown to have short carrier lifetimes; corresponding carrier diffusion lengths of a few micrometers have been measured. As a result, only charge carriers generated in or near the depletion region contribute to the photodiode's current [Ref. 7].

b. Radiation-Induced Damage Mechanisms in Photodiodes

The two fundamental radiation-induced damage mechanisms in photodiodes are an increase in the dark current and a degradation in cell responsitivity. The increase in the dark current is primarily due to the creation of radiation-induced defect sites in the bulk region of the semiconductor material. As discussed previously, this dark current is the primary factor that limits, for instance, the minimum signal that a photodiode can detect as a result of unwanted noise.

The radiation-induced reduction in the responsitivity of photodiodes results in a decrease of photocurrent gain (i.e., the ratio of output current, voltage or power to input current, voltage or power, respectively). Radiation reduces the carrier lifetimes by increasing the number of defect sites where carriers can recombine. If the transient time is much less than the carrier lifetime, only a small reduction in the gain results from the radiation-induced decrease in the carrier lifetime. However, if the lifetime of a carrier is originally comparable to the magnitude of the carrier transient time, the radiation-induced reduction in the photodiode's gain is significant.

Photodiodes are very susceptible to ionizing radiation damage as in the intense transient radiation pulses that accompany a nuclear weapon detonation. A large ionization-induced current is produced by the same mechanisms that cause photon-

induced currents to be generated under normal photodiode operating conditions. The large pulse of an ionization-induced current is usually more threatening to the more sensitive external detector circuits than to the photodiode. Unfortunately, the sensitivity of photodiodes to this type of radiation is heightened by their requirement for relatively large collective surface areas exposed to the environment to obtain maximum photopower [Ref. 7].

G. CHAPTER SUMMARY

This chapter described the effect radiation has on semiconductive devices and the difficulties discovered attempting to locate DLTS data for radiation-induced defect simulations.

The next chapter discusses techniques used to produce these defects in the SILVACO ATLAS$_{TM}$ software programs.

THIS PAGE INTENTIONALLY LEFT BLANK

V. SIMULATION

A. CHAPTER INTRODUCTION

This chapter describes the use of SILVACO ATLAS$_{TM}$ software as a light emitting diode and solar cell radiation-induced defect simulation tool.

B. SILVACO ATLAS$_{TM}$

Two 2D-simulations were created using the SILVACO ATLAS$_{TM}$ Virtual Wafer Fabrication software for this thesis research. This virtual software allows the user to graphically analyze the internal operation of semiconductor designs without having to go through the extensive process of growing, designing and testing semiconductive devices. It consists of interactive tools that can numerically simulate processing and electrical testing of semiconductive devices.

The simulation in SILVACO ATLAS$_{TM}$ was designed using the following modules from the suite: ATLAS$_{TM}$, DeckBuild$_{TM}$, TonyPlot$_{TM}$, DevEdit$_{TM}$ and LUMINOUS$_{TM}$. The following outline, Figure 5.1, illustrates the interconnecting relationship between the individual modules.

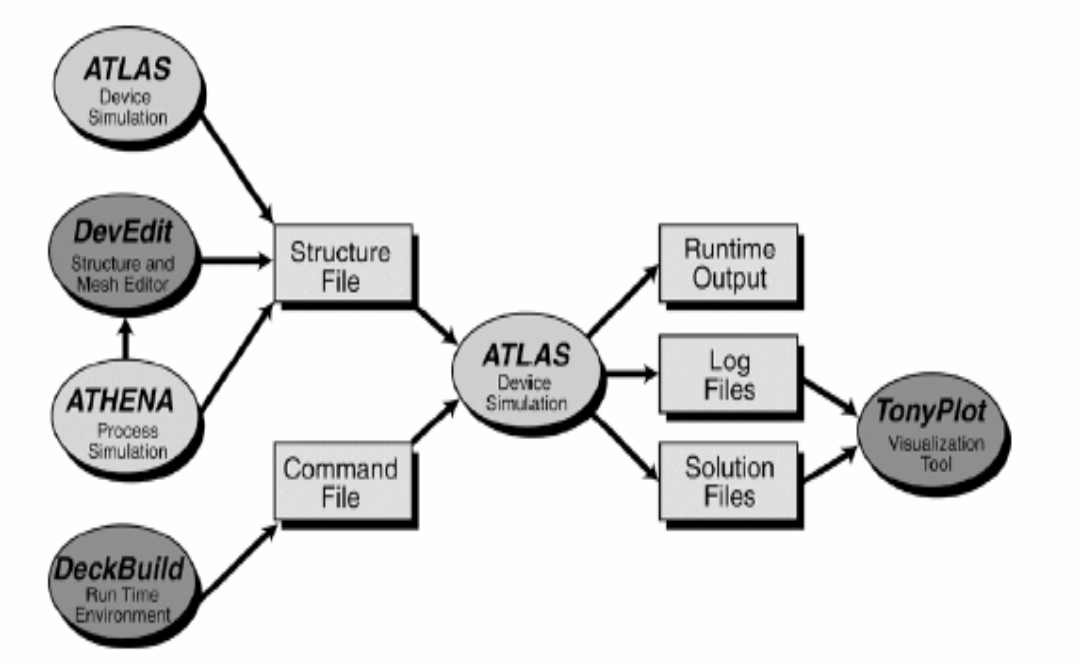

Figure 5.1. SILVACO ATLAS$_{TM}$ Input and Output Relationships [From Ref. 2.]

1. ATLAS$_{TM}$

ATLAS$_{TM}$ is a 2D/3D simulator for semiconductor devices. ATLAS$_{TM}$ can provide data and insights into the internal physical mechanisms of a device based on predicted electrical behavior. It is possible to use it either as a standalone tool or as a core unit for the SILVACO ATLAS$_{TM}$ Virtual Wafer Fabrication software environment [Ref. 2].

2. Deckbuild$_{TM}$

DeckBuild$_{TM}$ is an interactive graphical user interface to provide a user-friendly runtime environment for integration of the different aspects of the SILVACO ATLAS$_{TM}$ software suite. A control window is provided for file creation and control. Many of the features are automated to allow for accurate simulation in a simple to use environment. TonyPlot$_{TM}$ is the stand-alone program, possible to also reference in DeckBuild$_{TM}$, to display the results [Ref. 2].

3. DevEdit$_{TM}$

DevEdit$_{TM}$ is a device editor that can be used to generate a mesh for the structure designed in DeckBuild$_{TM}$ and ATLAS$_{TM}$. A limitation of device simulators prior to DevEdit was inadequate or poor structure meshes. DevEdit$_{TM}$'s usage was integrated into DeckBuild$_{TM}$ to allow for a more complete and accurate solution [Ref. 2].

4. LUMINOUS$_{TM}$

This general purpose Silvaco tool is a light absorption program integrated into the ATLAS$_{TM}$ framework to run with device simulation products. LUMINOUS$_{TM}$ calculates optical intensity profiles within the semiconductor device and converts these profiles into photo-generation rates in the device simulators. This tool allows the user to simulate electronic responses corresponding to various optical signals and wavelengths for a wide variety of optical detectors.

LUMINOUS$_{TM}$ was utilized in two different ways for this thesis. The first was to measure the luminescent light intensity created by the light emitting diode when applying current; the second was to simulate the optical light applied to the solar cell to create current.

C. SEMICONDUCTOR MODELING

Two SILVACO ATLAS$_{TM}$ models were generated for this thesis, one for the light emitting diode and another for the solar cell. The light emitting diode's model was derived from device parameters detailed in literature [Ref.15]. Basic understanding of the Naval Postgraduate School course, *Semiconductor Device Technologies*, and its literature was utilized to develop the solar cell's model [Refs. 3, 13].

In addition to understanding semiconductor device configuration and operation, a thorough understanding of SILVACO ATLAS$_{TM}$ and its limitations was needed in this thesis. Simulation data including trap energy levels, defect sizes, defect densities and defect charge amounts had to be understood as well as identified for successful implementation into the model simulations. As mentioned earlier, DLTS data extracted from nitrogen-irradiated GaAs semiconductors was implemented in the SILVACO ATLAS$_{TM}$ codes to simulate the radiation-induced defects.

Figure 5.2 shows the general process that was utilized to develop and implement simulated radiation-induced defects into the SILVACO ATLAS$_{TM}$ program models.

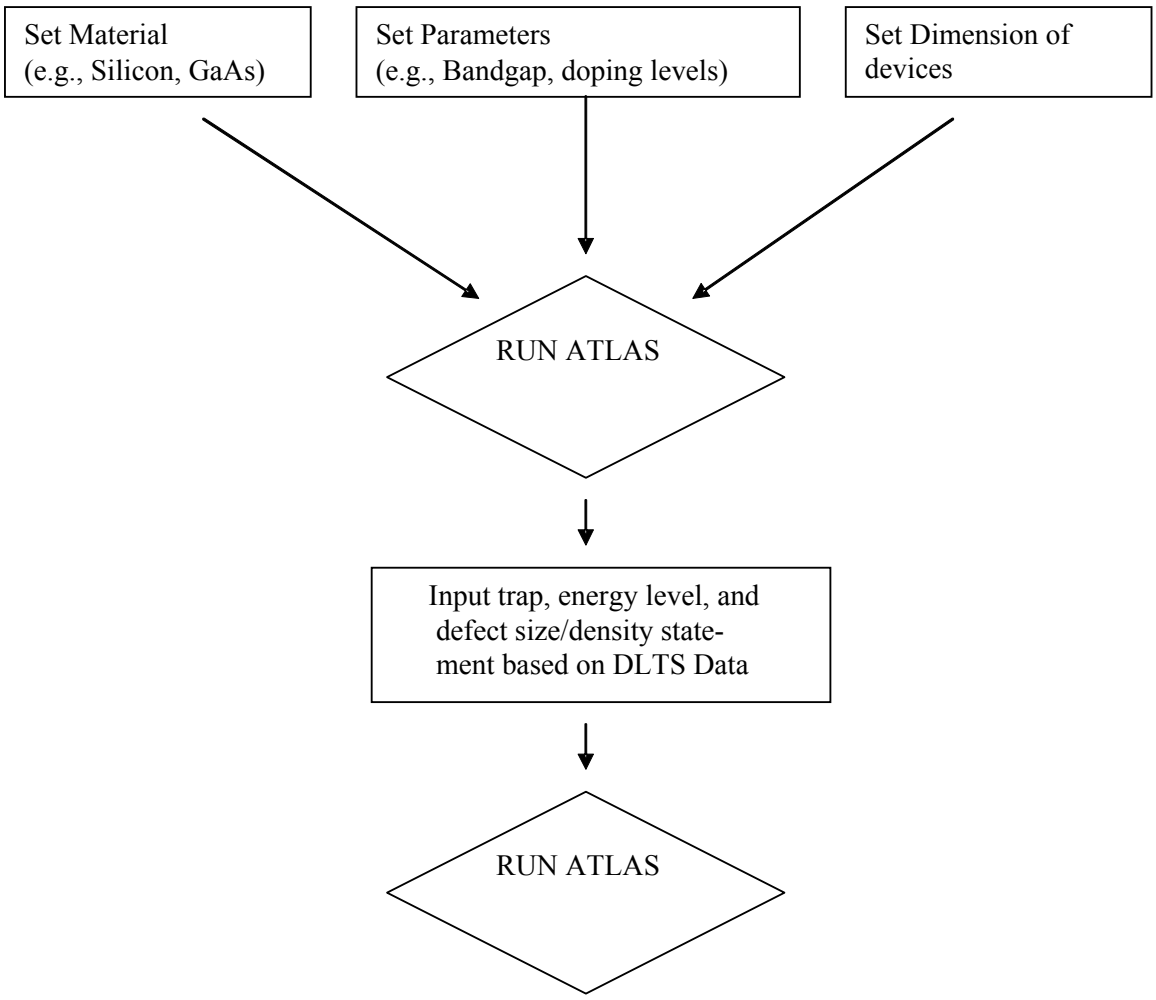

Figure 5.2. Flowchart of the SILVACO ATLAS$_{TM}$ Process

Implementing the defect energy levels, trap densities and trap sizes was found to be the most difficult aspect of this process because locating DLTS defect data sources was very challenging.

Follow-on sections provide illustrations and descriptions of the constructed simulation devices utilized in this thesis.

1. Solar Cell Model

Figure 5.3 illustrates the SILVACO ATLAS$_{TM}$ solar cell model results. The legend within the figure defines the solar cell's photogeneration rates. These are expressed using the log of the electron-hole pair generation rates that correspond to the color-coded display. For example the highest numerical value (e.g., 21.4) corresponds to the color-

coded horizontal layer that is generating $10^{21.4}$ electron-hole pairs per cm^3. This virtual perspective is very useful when designing the solar cell models because following simulation execution, an internal view of the cell's active operating regions can be instantly examined.

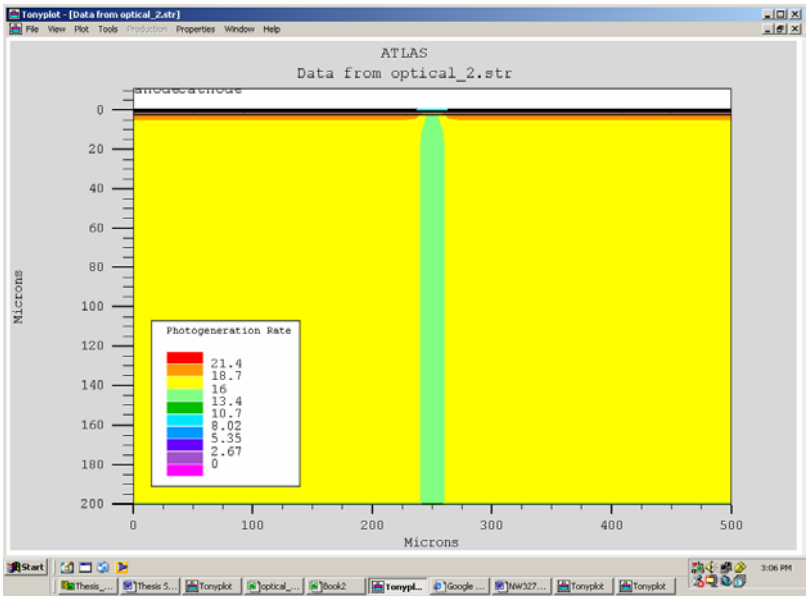

Figure 5.3. SILVACO ATLAS$_{TM}$ Solar Cell Model

Figure 5.3 is a two-dimensional, virtual-view of the constructed solar cell model. Since the cell's dimensions can be specified in SILVACO ATLAS$_{TM}$, this device was modeled to represent an actual solar cell with 200×500 micron dimensions. The very top portion of the vertical-band seen spanning in the middle of the model represents the upper metal contact of the semiconductive material. The thin strip along the horizontal bottom of the cell is the lower metal contact. The top and bottom metal contacts of the device are more appropriately termed the anode and cathode, respectively. These areas identify the power extraction points of the solar cell.

SILVACO ATLAS$_{TM}$ also allows the user to zoom in on model areas, enabling its users to examine specific regions of constructed models. Figure 5.4 shows a closer examination of device operation near the surface of the solar cell.

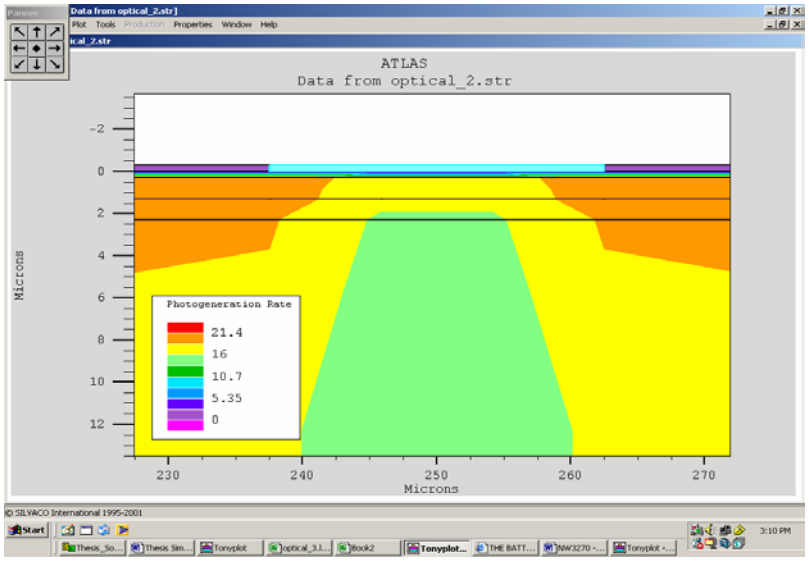

Figure 5.4. SILVACO ATLAS$_{TM}$ Solar Cell Model – A Closer Look

As seen in the figure, this closer view better illustrates the upper metal contact of the semiconductive material that is outlined by the light-blue, rectangular shaped region at the very top-center of the device. This closer examination also reveals that the photogeneration rate is significantly less directly beneath this metal contact region of the solar cell than the other regions. This is because the area directly beneath the electrical contact is blocked from the simulated solar light. The areas spanning out from the blocked region are observed to have increasing photogeneration rates. Most of the higher photogeneration rates are observed in the upper solar cell layers because a significant majority of the photon energy is absorbed here prior to reaching the remaining body (e.g., the yellow region) of the simulated device.

a. Power Calculations

Building on the information covered in the previous sections, we now discuss the solar cell's current and power relationships utilized in this thesis. The maximum power of the solar cell is given as the maximum current and voltage product of the cell's *I-V* curve. To determine the current per cm^2 of the constructed solar cell with no material defects implemented into the simulation models, the following relationship was developed

$$I_{MAX} \times 200,000 = J_{A/cm^2} \tag{5.1}$$

where the 200,000 scalar is the factor needed to convert the current generated by the constructed solar cell into ampere per cm^2; I_{MAX} is the maximum current derived from the *I-V* curve and J_{A/cm^2} is the current density.

Solutions derived from Equation 5.1 were used to determine the maximum output power of the constructed solar cell given by the following relationship

$$V \times J_{A/cm^2} = P_{MAX} \tag{5.2}$$

where P_{MAX} is the maximum output power density produced by the solar cell per cm^2.

Once the simulations were executed and their data was extracted, the numerical results obtained by utilizing both Equations 5.1 and 5.2 were then used to create the comparative *I-V* curve (Figure 6.5) and the power degradation curve (Figure 6.6) seen later in Chapter VI.

2. Light Emitting Diode Model

Figure 5.5 illustrates a two-dimensional, virtual-view of the light emitting diode model that was constructed using the SILVACO ATLAS$_{\text{TM}}$ software. The legend within the figure defines the device's semiconductor material make-up and corresponds to the color-coded display.

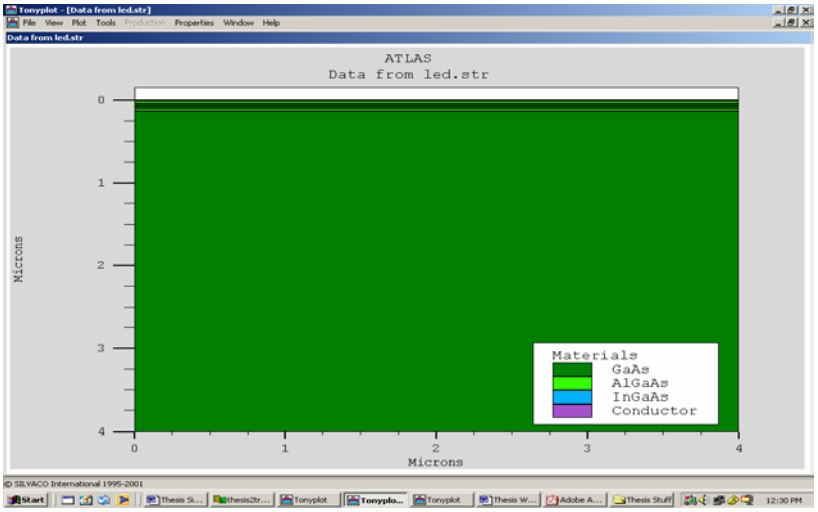

Figure 5.5. SILVACO ATLAS$_{\text{TM}}$ Light Emitting Diode Model

The model's dimensions are representative of a light emitting diode with 4×4 micron dimensions. It cannot be observed in the Figure 5.5 due to the extremely small dimensions of this device, but at its horizontal-top is the simulated upper metal contact of the semiconductive material and along its horizontal-bottom is the simulated lower metal contact. Again as with the solar cell, the top and bottom metal contacts of the device are more appropriately termed the anode and cathode, respectively. These metal contacts identify where power is applied to the device for subject illumination.

Figure 5.6 illustrates a closer look by zooming in on the device.

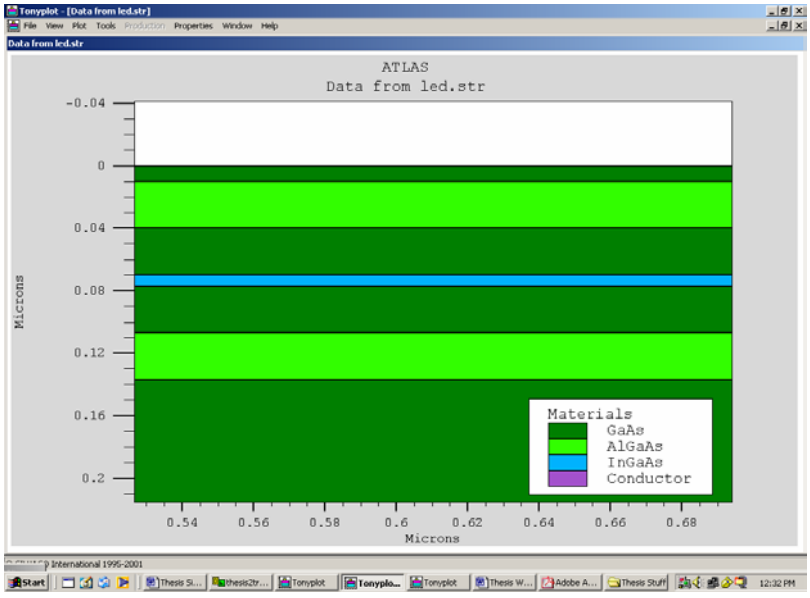

Figure 5.6. SILVACO ATLAS$_{TM}$ Light Emitting Diode Model – A Closer Look

As discussed previously in Chapter II, the thinnest layer of the device, the InGaAs layer (e.g. the blue layer), is the region where the electrons move across the n-type region, closer to the p-type region and recombine creating photons of luminous energy. This closer, zoomed-in view, also illustrates just how thin these virtual semiconductor layers are. The InGaAs layer is approximately only 0.01 micron in thickness.

D. DESIGN

1. Mesh Generation

Mesh design is an important factor to consider when designing semiconductors in SILVACO ATLAS$_{TM}$. The mesh intersections are designed by the simulation program-

mer to sufficiently cover the constructed device and are the data extraction points used to sample electrical characteristics of the model at designated intervals. It is often the requirement for accuracy and numerical efficiency that dictate the size of the sample intervals. Accuracy increases with finer grid points while numerical efficiency increases with fewer grid points. Since these simulations are computer driven programs, a finer grid equates to longer simulation runtime.

Figures 5.7 and 5.8 illustrate the SILVACO ATLAS$_{TM}$ solar cell and the light emitting diode mesh models, respectively.

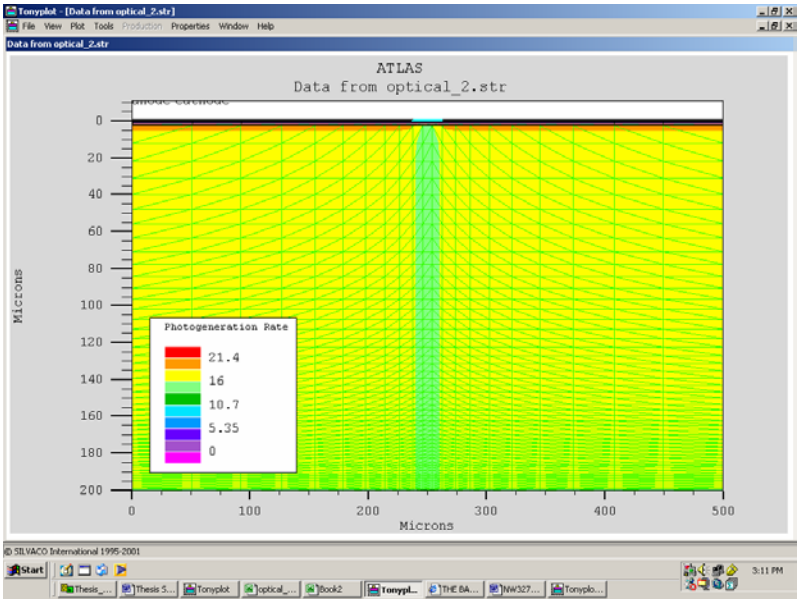

Figure 5.7. SILVACO ATLAS$_{TM}$ Solar Cell Mesh Model

Examining Figure 5.7, it is seen that the entire structure is thoroughly sampled at designated intervals. Depending on the complexity of device design, some areas may require more sampling than others to sufficiently sample all the electrical activity created by the *recombination* and *generation* processes occurring within the device.

Figure 5.8 illustrates the mesh model of the constructed light emitting diode.

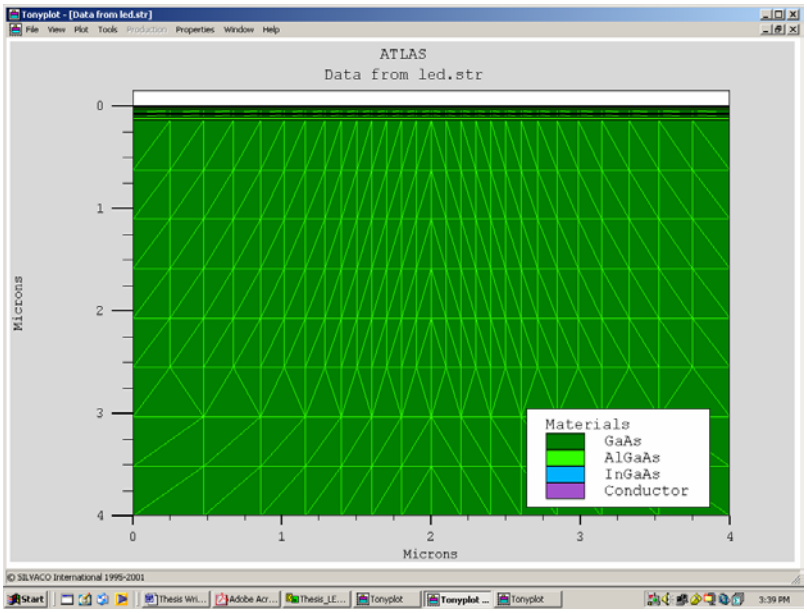

Figure 5.8. SILVACO ATLAS$_{TM}$ Light Emitting Diode Mesh Model

As mentioned for the solar cell, examining the above device it is seen that the structure is thoroughly sampled at designated intervals.

The mesh models for the light emitting diode as well as the solar cell were briefly included in these previous sections to offer visual representations of how SILVACO ATLAS$_{TM}$ analytically samples the constructed semiconductive devices to derive its simulation results. For this thesis, determination of appropriate sampling intervals was achieved, in general, through trial and error. The objective was straightforward; electrically sample the devices effectively but refrain from oversampling, resulting in long and unnecessary simulation runtime.

E. SIMULATION OF RADIATION DAMAGE

The SILVACO ATLAS$_{TM}$ software enables the user to simulate radiation-induced damage by utilization of the trap statement, which activates bulk traps at discrete energy levels within the bandgap of the semiconductor material. An example of the trap statement as written in simulation code is given below and is followed by a line by line explanation of terms:

Example line 1 – material material=GaAs region=2 taun0=1e-8 taup0=1e-8 mun0=13800 mup0=240

Example line 2 – trap region=2 e.level=1.6 acceptor density=1.507e13 degen=2 \ sign=6.45e-19 sigp=6.45e-14

Line 1 designates the subject semiconductive material being modified (e.g., material = GaAs) as well as which corresponding layer within the constructed device that material is located (e.g., region = 2). For instance, referring back to Figure 5.6's observed thinnest layer, the material would be defined as InGaAs and, if numbering the figure's layers sequentially from top to bottom, the region would be designated as 4. Region designation of all constructed device layers is established by the simulation programmer and must remain consistent throughout the SILVACO ATLAS$_{TM}$ program code. Next in line 1, the Shockley-Read-Hall (SRH) lifetime of the electrons and holes of the specified material are defined (e.g., taun0 $= 1\times10^{-8}$ s and taup0 $= 1\times10^{-8}$ s respectively). Finally in line 1, the electron and hole mobility rates of the specified material are also defined (e.g., mun0 $= 13,800$ cm^2/V-s and mup0 $= 240$ cm^2/V-s, respectively).

Line 2 designates which region of the constructed device the simulated trap is placed (e.g., region = 2). Next, the trap's energy level within that region's bandgap is defined (e.g., e.level = 1.6). Next, programmers can specify if the simulated trap is a donor type or an acceptor type trap while defining its defect density (e.g., acceptor density $= 1.507\times10^{13}$ per cm^3). Next, the degeneracy factor of the trap level is specified (e.g., degen = 2). This factor is utilized by the internal computations of the SILVACO ATLAS$_{TM}$ program to numerically incorporate trap parameters into its output response. The subject degeneracy factor of 2 used in this thesis was extracted from SILVACO ATLAS$_{TM}$ simulation code found in similar defect research work, Reference 7. Finally in line 2, users can specify the capture cross-section of the trap for electrons and holes (e.g., sign $= 6.45\times10^{-19}$ cm^2 and sigp $= 6.45\times10^{-14}$ cm^2, respectively).

Further information regarding any of the trap parameters discussed above can be found in Reference 2, the SILVACO ATLAS$_{TM}$ Users Manual.

F. CHAPTER SUMMARY

This chapter discussed the technical aspects of utilizing the commercially available SILVACO ATLAS$_{TM}$ virtual software to achieve the objectives of this thesis.

The next chapter will provide comparative results of the SILVACO ATLAS$_{TM}$ and NIEL predictions.

VI. RESULTS

A. CHAPTER INTRODUCTION

Simulations were conducted after radiation-induced defects were implemented into the SILVACO ATLAS$_{TM}$ programs. Microsoft Excel and the commercially available software package, MATLAB, were both then utilized to graphically compare the program's simulation predictions with the results of NIEL predictions (e.g., MATLAB implementation is discussed in Appendix B). This chapter presents these results and provides further discussion to explain how the SILVACO ATLAS$_{TM}$ computer-based program can be offered as a valid radiation-induced defect prediction method.

B. RADIATION MODELING

1. Modeling Radiation-Induced Defects

In this thesis, simulation of radiation-induced defects was achieved by adding defects to the model within the trap statements. To achieve this for the light emitting diode, the size of the trap's capture cross-section was varied. Similarly for the solar cell, the amount of acceptor-trap defect densities was varied. Table 6.1 shows the values used in this statement.

	Fluence (cm^{-2})	E_T **(eV)**	σ_n **(cm^2)**	N_t
E2	1×10^{12}	0.084	3.39×10^{-K}	2.214×10^{-K}
E5	1×10^{12}	0.763	1.33×10^{-K}	1.692×10^{-K}

Table 6.1. Irradiation Defects for Solar Cell Simulation [From Ref. 21.]

These values were taken from Reference 21 and then implemented into the SILVACO ATLAS$_{TM}$ program models. In Table 6.1, *Fluence* represents the amount radiation energy, E_T is the activation energy levels, σ_n is the apparent donor capture cross-section of the created traps and N_t is the apparent trap density per cm^3.

For both σ_n and N_t, K was chosen as a random variable to simulate a range of varying radiation exposure amounts and has no other meaning. In the SILVACO ATLAS$_{TM}$ code, this parameter was varied linearly to represent changing density amounts and capture cross-section sizes to achieve simulation of changing radiation defect levels. To achieve this for σ_n, the apparent donor capture cross-section was varied in 15 linear increments from 3.39×10^{-25} cm^2 to 3.39×10^{-10} cm^2 for E2 placed defects and from 1.33×10^{-25} cm^2 to 1.33×10^{-10} cm^2 for E5 placed defects. Similarly for N_t, the apparent trap density was varied in 15 linear increments from 2.214×10^{10} to 2.214×10^{25} per cm^3 for E2 place defects and from 1.692×10^{10} to 1.692×10^{25} per cm^3 for E5 placed traps. Fluence level was kept constant at 1×10^{12} cm^{-2} throughout the simulations.

The E5 placed defects did not have any significant effect on device output responses and were not investigated further after simulations were conducted. As seen later Figure 6.5, the E2 placed defects were observed to have an effect on device output responses and were investigated further.

a. Trap Density and Capture Cross-Section Relating to Radiation-Fluence

When discussing radiation-induced defects, the relationships between trap density, trap capture cross-section and radiation fluence are shown to be directly related. The amount of fluence depends on the level of radiation energy to which the semiconductive material is exposed. The defects caused by this subject radiation create traps. The size of the trap's capture cross-section determine the extent of damage caused in the material. Destructive amounts of this energy begin to create increasing numbers of these defective traps. As trap density increases within the material, changes to its characteristics become more apparent, resulting in cell degradation.

2. SILVACO ATLAS$_{TM}$ and Non-Ionizing Energy Loss (NIEL) Comparisons

One of the objectives of this thesis was to compare NIEL predictions to the radiation-induced defect predictions using the SILVACO ATLAS$_{TM}$ software models.

a. Non-Ionizing Energy Loss (NIEL)

NIEL is the energy a particle imparts to a solid through mechanisms other than ionization. In general, it is the rate at which energy is lost to nonionizing events. Its calculations require information regarding the differential cross-section for atomic displacements ($d\sigma/d\Omega$), the average recoil energy of the target atoms (T) and a term which partitions the energy into ionizing and non-ionizing events called the Lindhard partition factor, (L). NIEL can be written as an integral over a solid angle given by the following relationship

$$\mathrm{NIEL(E)} = \frac{N}{A}\int_{\theta_{\min}}^{\pi}\left(\frac{d\sigma(\theta,E)}{d\Omega}\right)T(\theta,E)L[T(\theta,E)]\,d\Omega \tag{6.1}$$

where N is Avogadro's number, A is the atomic mass and $\theta_{\min}$ is the scattering angle for which the recoil energy equals the threshold for atomic displacement [Ref. 22].

NIEL can be calculated for electron damage and proton damage. Although the NIEL approach has wide application, published calculations are limited with respect to types of semiconductor materials, radiation types and energy levels because calculations over large energy ranges for NIEL predictions are not straightforward. They can involve coulombic, nuclear elastic and spallation (e.g., nuclear inelastic) interactions. Nevertheless, over the years these predictions have been useful in correlating displacement damage effects in semiconductive materials [Refs. 19, 22].

Figure 6.1 illustrates comparative graphs of NIEL and LED predictions for minority carrier lifetime coefficient damage taken from Reference 19.

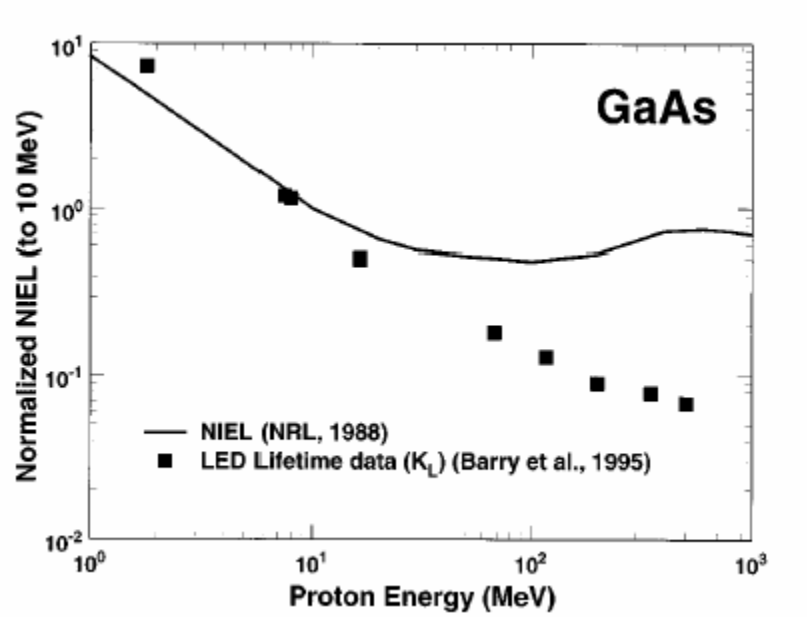

Figure 6.1. Minority Carrier Lifetime Coefficient Damage [From Ref. 19.]

As seen in Figure 6.1, NIEL predictions showing relative damage coefficients are higher than the LED lifetime data predictions at higher proton energies. Similar comparisons with other radiation prediction methods have also been shown to have higher NIEL damage coefficients at higher energy levels. A continuing debate exists concerning why these higher energy discrepancies occur [Ref. 19].

b. SILVACO ATLAS$_{TM}$ Versus NIEL

NIEL uses known displacement damage predictions to develop curves that generally show how the semiconductive characteristics will behave when exposed to radiation. To compare the NIEL predictions to the SILVACO ATLAS$_{TM}$ simulation predictions, curves were generated illustrating how photo-power and luminous intensity for the solar cell and the light emitting diode, respectively, varied as the radiation intensities were simulated to have been increased.

(1) Light Emitting Diode Comparisons. As a function of proton fluence for different proton energies, the plotted response of the normalized light output intensity of an InGaAs/GaAs Quantum-Well (QW) light emitting diode, Figure 6.2, was taken from Reference 15 and then compared to a graphical illustration, Figure 6.3, of

the luminous output power results derived from the SILVACO ATLAS$_{TM}$ light emitting diode simulation model as its donor trap cross-sections (sign) were increased linearly.

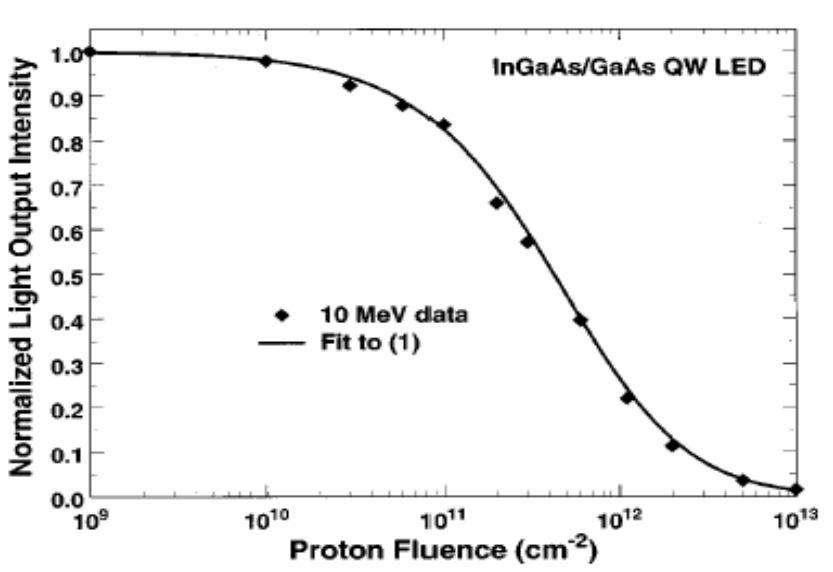

Figure 6.2. LED Luminous Output Power While Increasing Proton Fluence [From Ref. 15.]

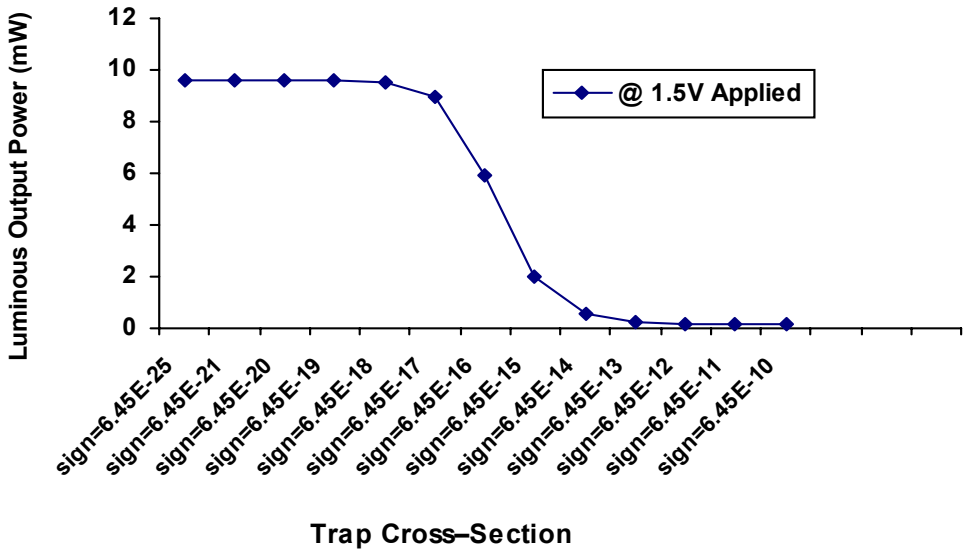

Figure 6.3. LED Luminous Output Power While Increasing Defect Trap Cross-Section

Figure 6.2 illustrates the response of the InGaAs/GaAs Quantum-Well (QW) light emitting diode when irradiated with increasing levels of 10 MeV proton fluences and Figure 6.3 illustrates a similar effect when the donor trap cross-sections of the SILVACO ATLAS$_{TM}$ light emitting diode model were increased linearly in 15 increments from 6.45×10^{-25} cm^2 to 6.45×10^{-10} cm^2. In these comparisons, the 10-MeV proton fluences in Figure 6.2 represent the environment's radiation that causes the induce defects in the semiconductive material; and, similarly in the SILVACO ATLAS$_{TM}$ program, increasing the donor trap cross-sections is representative of the net-effect of increased radiation levels (i.e., increased radiation levels causes more traps and increases their cross-section).

A 50% normalized light degradation point is observed in Figure 6.2 at a proton fluence of approximately 3×10^{11} cm^2. At this proton fluence level, half of the light emitting diode's luminous light has been degraded. Comparatively looking at the 50% luminous degradation point in Figure 6.3, the SILVACO ATLAS$_{TM}$ code had a trap cross-section of approximately 6.45×10^{-16} cm^2 with a constant density of 1×10^{19} traps per cm^3. Referring back to Table 6.1, the E5 trap's cross-section is larger than the E2 trap's cross-section and was shown to have a greater effect on device properties. The E5 trap has a cross-section of 1.33×10^{-15} cm^2 which is an order of magnitude lower than in the 50% light output cross-section seen in Figure 6.3. Therefore, the true trap density should also be an order of magnitude lower as well, giving a trap density of 1×10^{18} traps per cm^3, vice 1×10^{19} traps per cm^3. From these comparisons, a proton fluence of approximately 3×10^{11}cm^{-2} is equivalent to a trap density of 1×10^{18} E5 traps per cm^3.

As discussed previously, to achieve these results in this thesis, the trap density was not varied in the simulations and was set to 1×10^{19} traps per cm^3. The acceptor cross-section also remained constant and was set to 6.45×10^{-14} cm^2. Only the donor cross-section was varied to achieve the results illustrated in Figure 6.3.

Recommendations for future work would be to keep the trap cross-sections constant and vary the trap densities and acceptor cross-sections to explore this correlation to the irradiation comparisons as well.

(2) Solar Cell *I-V* Curve Comparisons. Figure 6.4 was derived from calculations of the solar cell's current and voltage measurements, as discussed previously in Chapter IV to produce the constructed model's *I-V* curve. Figure 6.4 illustrates the solar cell's *I-V* curve with no defects yet implemented into the simulation software.

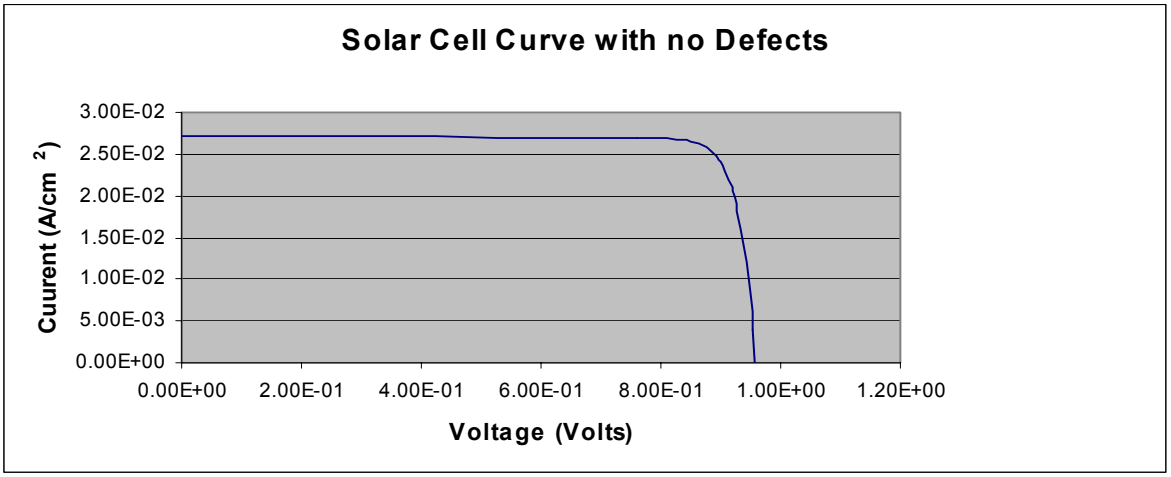

Figure 6.4. Modeled Solar Cell *I-V* Curve with No Defects

Implementing the defect data obtained from Reference 21 and increasing the acceptor-trap defect densities linearly until degradation was observed, produced Figure 6.5.

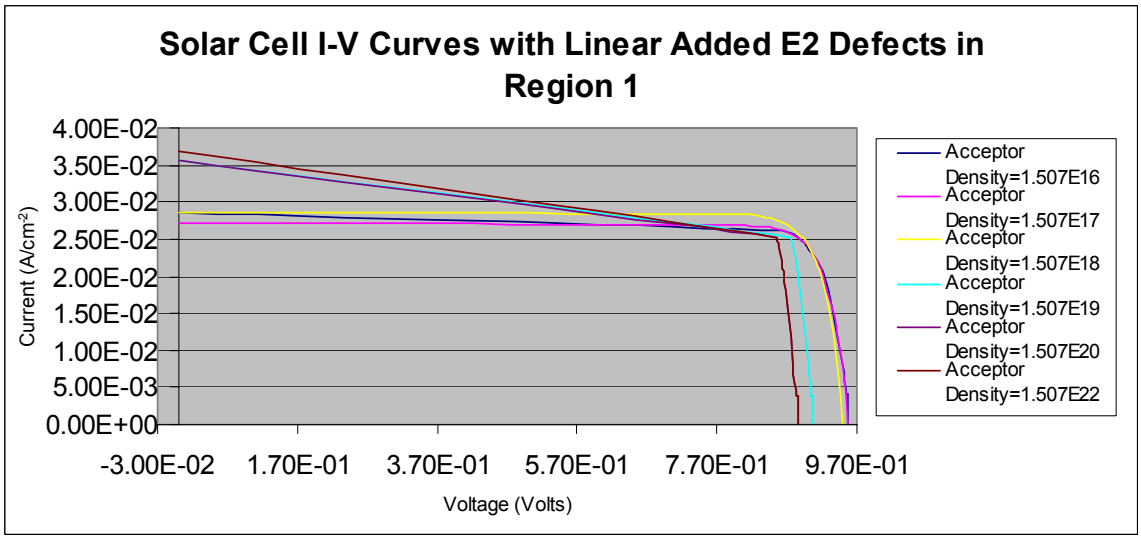

Figure 6.5. *I-V* Curve Degradation As a Result of E2 Defect Placed in Region 1 of the Solar Cell

Figure 6.5 illustrates the constructed solar cell's response when defect E2 was placed into Region 1 of the structure. Acceptor-trap defect densities were increased linearly to simulate increasing irradiation levels. When the acceptor-trap density was lower than 1.507×10^{18} traps per cm^3, no *I-V* curve changes were observed. The next extreme, when the acceptor-trap density was increased higher than 1.507×10^{23} traps per cm^3, further *I-V* curve changes could not be observed. At these higher levels, the results seem to produce a flawed graph because the curved knee disappears and becomes an angled knee. It was concluded that at this point the solar cell is effectively "dead" and/or has reached its maximum radiation tolerance. This may be due to insufficient data points taken or possibly because the model used to derive the radiation predictions in the SILVACO ATLAS$_{TM}$ simulation code was incapable of resolving the internal arrhythmic operations of the constructed solar cell at such high trap densities.

The data results found in the Microsoft Excel files that produced Figure 6.5 were also extracted to produce Figure 6.6 by utilizing the solar cell power equation discussed in Chapter IV, Equation 5.1. Figure 6.6 illustrates the power degradation curve of the constructed solar cell as acceptor-trap defect densities were increased linearly to simulate increasing irradiation levels.

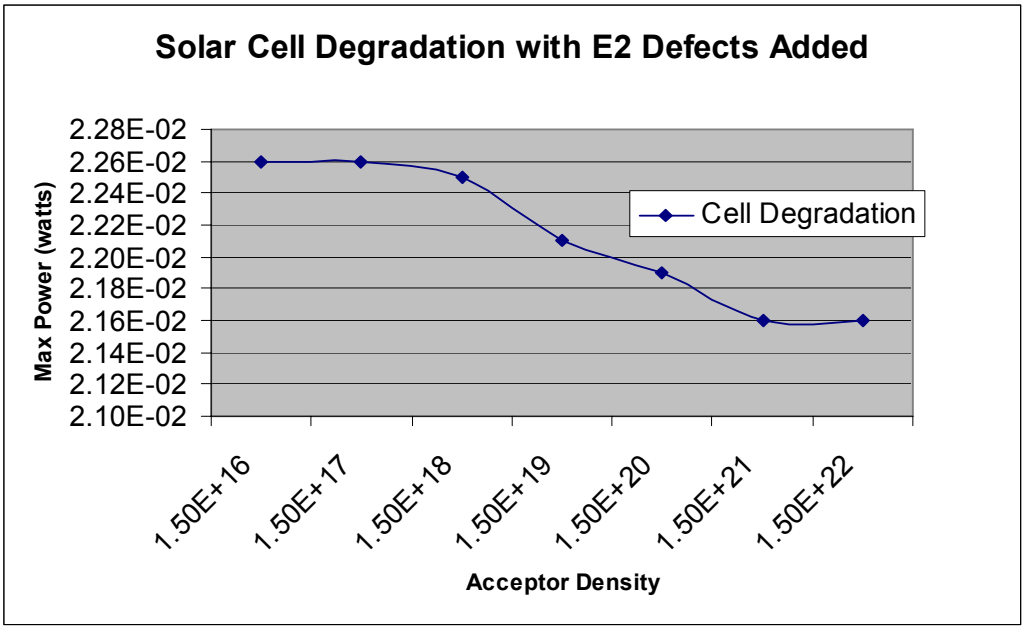

Figure 6.6. Power Degradation As a Result of E2 Defect in Region 1 of the Solar Cell

These results indicate that cell power degraded linearly as defect density increased linearly. This correlation establishes the validity of this process and demonstrates cell degradation prediction. Not yet as accurate, this process can be related to the NIEL predictions seen in Figure 6.1. Both curves follow the same general slopes until higher irradiation energies are reached.

3. Model Limitations

This process requires much more robust, comprehensive research. More DLTS data derived from studies on the similar semiconductive materials is required to improve the accuracy of the SILVACO ATLAS$_{TM}$ radiation predictions.

It must also be noted that while trying to reproduce the same results found in Reference 21 by implementing defect data in the SILVACO ATLAS$_{TM}$ trap statements, the acceptor capture cross-section of the defect had to be made very small, 1×10^{-30} cm^2, in order to simulate that a *p*-type defect was not present in the material. This was necessary because only *n*-type defects appeared in the research work utilized to obtain the defect data use in this thesis, Reference 21.

C. CHAPTER SUMMARY

This chapter provided results and comparisons for the SILVACO ATLAS$_{TM}$ and NIEL predictions. A review of the findings concluded that these radiation prediction methods compared favorably enough to warrant further studies and research.

The next and final chapter presents a summary of the work and recommendations for future study.

THIS PAGE INTENTIONALLY LEFT BLANK

VII. CONCLUSION

A. SUMMARY OF WORK

This thesis generated SILVACO ATLAS$_{TM}$ radiation-induced defect predictions for a light emitting diode and a solar cell, discussed the processes for modeling these devices, and made comparisons between the SILVACO ATLAS$_{TM}$ and NIEL radiation predicting methods. The research conducted for this thesis concludes that the SILVACO ATLAS$_{TM}$ Virtual Wafer Fabrication software could be offered as a valid substitution for future radiation-induced damage predictions.

Progress was made in this thesis but additional research is required. Assumptions were made to compensate for the lack of DLTS data that was needed to deliver more robust models of the radiation defects. This thesis is intended to be part of a larger study that will lead to the cost-effective simulation of radiation-induced defects in semiconductor devices using a computer-based program vice having to grow, irradiate and test these materials. Once this process has matured and more DLTS data has been explored, it will prove to be an essential time- and money-saving semiconductor radiation-prediction simulation tool. Even with the limited DLTS data implemented in this current research, this process has shown to be both a versatile and a reliable method for predicting radiation-induced defects.

Military systems as well as civilian systems often must be capable of sustained operation in environments containing sources of both natural and man-made radiation. Initiatives to predict these effects on today's electronics will continue to grow as technology becomes more and more reliant on semiconductive materials. This thesis delivers one such radiation prediction initiative that, when matured fully, will be one of the most reliable and cost-effective radiation damage prediction tools available to the modern electronics industry.

B. ALTERNATE FUTURE ANALYSIS

This thesis has made progress in this area of research but other areas need further exploration to increase understanding of how to simulate and predict semiconductor degradation in a computer-based program more effectively. The following are three areas of concern:

- The overall accuracy of these simulated radiation defects has to be increased. This can be achieved by conducting a series of SILVACO ATLAS$_{TM}$ tailored experiments where DLTS data is extracted specifically for program parameters. These results should be implemented into the SILVACO ATLAS$_{TM}$ codes to enhance the accuracy of simulated radiation-induced defects.
- Devices modeled should be of similar dimensions and material make-up from which the DLTS studies are derived. One recommendation would be to start with a pre-manufactured device and then to model it in SILVACO ATLAS$_{TM}$ and irradiate it with incremental energy levels, getting the SILVACO ATLAS$_{TM}$-tailored DLTS data after each progressing irradiation level to finally be implemented into program models.
- Aging is also a factor in all semiconductors. Semiconductors degrade when they are forward biased for long periods of time and most manufacturers list degrading curves as a result. No studies were discovered that determined whether radiation and aging are interdependent. Known applications and available research assume that they are independent of one another. Future analysis should look at aging effects to determine how much it plays a role in semiconductor degradation vice or in addition to radiation-induced damage.

APPENDIX A. GUIDE TO REPRODUCING SILVACO ATLAS$_{TM}$ RESULTS [AFTER REF. 23]

This appendix becomes useful when attempting to reconstruct the simulation model results without having to start from the very beginning. This appendix provides the methods used to reproduce the SILVACO's ATLAS$_{TM}$ simulation results as mentioned in previous thesis work, Reference 23, as well as the actual software simulation codes developed for the solar cell and light emitting diode.

A. REPRODUCING SILVACO ATLAS$_{TM}$ RESULTS

SILVACO's ATLAS$_{TM}$ semiconductor software is a powerful and very capable tool in deciphering the electrical and material properties of a semiconductor. The vast array of built-in functions and add-on modules create a powerful tool with a steep learning curve. This concise section will attempt to help create a standardize method to collect, organize, and extract the data from Silvaco for further analysis.

The process begins with the DeckBuild$_{TM}$ graphical user interface and the creation of an input file. ATLAS$_{TM}$ is the module used in this research and the module is adequate and effective for all of the work that was accomplished. The physical parameters and structural dimensions were set for the input file; to be used globally throughout the model, in conjunction with a doping level and *MODEL* command setting. In the *MODEL* command, the lattice temperature is set for the ATLAS$_{TM}$ run. At this point, the program is ready to enter the recording stage of the process.

The *PROBE* function was used extensively to gather the data required for proper analysis. This function was used to record the temperature, the hole concentration, and the electron concentration. An iterative stepping of minimal bias is applied to allow for the software to calculate the properties of the material. The *STRUCTURE* (.STR) file is saved and the probed values are logged into a *LOG* (.log) file. At this point, the program is ready to quit the ATLAS$_{TM}$ run at the given temperature and begin stepping on to the next temperature to begin the process anew. The new temperature is set in the MODEL command. The *LOG* file is then appended to record the new data from the updated temperature. The process repeats itself until the *QUIT* command is called to end the process.

It is then possible to export this raw data into Microsoft Excel or MATLAB to be further categorized and analyzed.

B. SOURCE CODES

These codes simulate a GaAs derived solar cell and light emitting diode, respectively. The radiation-induced defects are implemented into the constructed simulation device models by utilization of the trap statement.

SOLAR CELL SOURCE CODE

```
go atlas
title SOLAR CELL Simulation

mesh smooth=1 space.mult=1
#*********************************************************************
#                           MESH GENERATION
#**********************      DEMISIONS     ***************************
#                           10 um X 500 um
#*********************************************************************
# X-Mesh:  surface=500 um2 = 1/200,000 cm2
x.mesh loc=-250 spac=50
x.mesh loc=0 spac=10
x.mesh loc=250 spac=50

# Y-Mesh
# Vacuum
y.mesh loc=-0.1 spac=0.01
# Emitter (0.1 um)
y.mesh loc=0 spac=0.01
# Base (3 um)
y.mesh loc=10 spac=1

#*********************************************************************
#                              REGIONS
#*********************************************************************
# Emitter
region num=1 material=GaAs x.min=-250 x.max=250 y.min=-0.1 y.max=0
# Base
region num=2 material=GaAs x.min=-250 x.max=250 y.min=0 y.max=10
#*********************************************************************
#                           ELECTRODES
#*********************************************************************
electrode name=cathode x.min=-250 x.max=250 y.min=-0.1 y.max=-0.1
electrode name=anode x.min=-250 x.max=250 y.min=10 y.max=10
#*********************************************************************
#                           DOPING LEVELS
#*********************************************************************
# Emitter
doping uniform region=1 n.type conc=2e18
# Base
doping uniform region=2 p.type conc=1e17
```

```
#*****************************************************************
#                          MATERIAL SPECS
#*****************************************************************
material TAUN=1e-7 TAUP=1e-7 COPT=1.5e-10 AUGN=8.3e-32 AUGP=1.8e-31

# Vacuum
material material=Vacuum real.index=3.3 imag.index=0

# GaAs
material material=GaAs EG300=1.42 PERMITTIVITY=13.1 AFFINITY=4.07
material material=GaAs MUN=8800 MUP=400
material material=GaAs NC300=4.7e17 NV300=7e18
material material=GaAs index.file=GaAs.opt

#*****************************************************************
#                          RADIATION DAMAGE SIMULATION
#*****************************************************************
material material=GaAs region=4 taun0=1e-8 taup0=1e-8 mun0=13800
mup0=240
#E2
#trap region=2 e.level=0.084 acceptor density=1.507e19 degen=2 \
#sign=3.32e-21 sigp=2e-40
#E5
trap region=1 e.level=.763 acceptor density=1.692e19 degen=2 \
sign=1.33e-15 sigp=2e-40

#*****************************************************************
#                          NUMERICAL METHODS
#*****************************************************************
models BBT.KL TATUN TRAP.TUNNEL
#model fermi conmob fldmob srh print
output val.band con.band recomb traps

#*****************************************************************
#                          LIGHT BEAM
#*****************************************************************
beam num=1 x.origin=0 y.origin=-5 angle=90 \
      power.file=AM0silv.spec wavel.start=0.21 wavel.end=4 wavel.num=50
#*****************************************************************
#                      SOLUTION SPECIFICATION
#**********************                    ************************
#                          Spectral Response
#*****************************************************************
solve init

method gummel maxtraps=10 itlimit=25
solve b1=0.9

method newton maxtraps=10 itlimit=100
solve b1=1
contact name=cathode current

struct outfile=optical.str
save outf=optical_2.str
#tonyplot optical_2.str -set optoex08_2.set
```

```
log outfile=optical_3.log
solve b1=1
solve icathode=1.26e-7 b1=1

solve icathode=1.24e-7 b1=1
solve icathode=1.22e-7 b1=1
solve icathode=1.2e-7 b1=1
solve icathode=1.1e-7 b1=1
solve icathode=1.0e-7 b1=1
solve icathode=0.8e-7 b1=1
solve icathode=0.6e-7 b1=1
solve icathode=0.4e-7 b1=1
solve icathode=0.2e-7 b1=1
solve icathode=0      b1=1

log off
#tonyplot optical_3.log
#tonyplot optical_2.log -set optoex08_3.set

quit
```

LIGHT EMITTING DIODE (LED) SOURCE CODE

```
go atlas
title LED Simulation

mesh smooth=1 space.mult=1.0
#*************************************************************
#                          MESH GENERATION
#**********************      DEMISIONS     ***********************
#                           4 um X 4 um
#*************************************************************
x.mesh l=0.0  spacing=0.25
x.mesh l=1.5  spacing=0.1
x.mesh l=2.5  spacing=0.1
x.mesh l=4.0  spacing=0.25

y.mesh l=0.0  spacing=0.02
y.mesh l=0.01  spacing=0.1
y.mesh l=0.040  spacing=0.1
y.mesh l=0.070  spacing=0.02
y.mesh l=0.077  spacing=0.1
y.mesh l=0.107  spacing=0.5
y.mesh l=0.137  spacing=0.5
y.mesh l=4.0  spacing=0.5

eliminate y.direction x.min=0.0 x.max=4.0 y.min=3.0 y.max=4.0
#*************************************************************
#                            REGIONS
#*************************************************************
region num=1 Material=GaAs   x.min=0.0   x.max=4  y.min=0.0 y.max=0.01
region num=2 Material=AlGaAs x.min=0.0   x.max=4  y.min=0.01
y.max=0.040
```

```
region num=3 Material=GaAs   x.min=0.0   x.max=4  y.min=0.040
y.max=.070
region num=4 Material=InGaAs x.min=0.0   x.max=4  y.min=.070 y.max=.077
x.comp=0.53
region num=5 Material=GaAs   x.min=0.0   x.max=4  y.min=.077 y.max=.107
region num=6 Material=AlGaAs x.min=0.0   x.max=4  y.min=.107 y.max=.137
region num=7 Material=GaAs   x.min=0.0   x.max=4  y.min=.137 y.max=4

elec   num=1  name=anode x.min=1.5 x.max=2.5 y.min=0.0 y.max=0.0
elec   num=2  name=cathode bot

#*****************************************************************
#                          DOPING PROFILES
#*****************************************************************

doping conc=4.0e18 p.type x.left=1.5 x.right=2.5 gaus char=0.5 ra-
tio.lat=0.6
doping uniform region=1 p.type conc=1.e25
doping uniform region=2 p.type conc=1.e19
doping uniform region=3 p.type conc=1.e20
#doping uniform region=4 p.type conc=1.e15
#doping uniform region=5 n.type conc=1.e05
doping uniform region=6 n.type conc=1.e14
doping uniform region=7 n.type conc=1.e19

#*****************************************************************
#                    RADIATION DAMAGE SIMULATION
#*****************************************************************

material material=InGaAs region=4 taun0=1e-8 taup0=1e-8 mun0=13800
mup0=240
trap region=3 e.level=1.6 acceptor density=1e19 degen=2 \
sign=6.45e-19 sigp=6.45e-14
#trap region=1 e.level=0.35 acceptor density=1e19 degen=2 \
#sign=2.65e-15 sigp=2.65e-25

#*****************************************************************
#                       NUMERICAL METHOD
#*****************************************************************

model auger optr srh bgn print
output con.band val.band recomb u.srh u.aug u.rad traps

#*****************************************************************
***
#                      SOLUTION SPECIFICATION
#**********************                        ************************
#                           RAMP VOLTAGES
#*****************************************************************
solve init
log outfile=light.log
method newton climit=1e-4 maxtrap=10
solve  l.wave=0.8 vanode=1 vstep=0.01 vfinal=1.5 name=anode
save outfile=light.str
log off
```

```
tonyplot light.log


solve init
log outfile=led.log
method newton
solve  vanode=1 vstep=0.05 vfinal=1.5 name=anode
save outfile=led.str
log off
tonyplot led.str
tonyplot led.log

#*************************************************************************
#                           LUMINOUS EXTRACTION
#*************************************************************************
measure u.radiative
measure u.total
quit
```

APPENDIX B. MATLAB UTILIZATION

This appendix provides discussion regarding the utilization of another commercially available software program, MATLAB, to graphically illustrate radiation predictions. This appendix also contains the source codes for the MATLAB displog and plotlog functions that were used in this thesis. These MATLAB codes are utilized to extract values from the SILVACO ATLAS$_{TM}$ output files, to execute defined numerical computations and then to graphically display their derived solutions.

A. EXCHANGING DATA WITH MATLAB

SILVACO ATLAS$_{TM}$'s TonyPlot illustrations are very useful tools but often the need exists to exchange data between other programs such as MATLAB. This thesis made use of MATLAB codes developed in previous thesis work, Reference 4, to create *I-V* curves displaying the semiconductor device responses resulting from radiation-induced defects implemented into the simulation models.

The MATLAB displog and plotlog functions utilized in this thesis are given by the following source codes:

DISPLOG SOURCE CODE

```
% (c) 2003 by D. C. Gladney----- displog function written in 2001 by
% P. Michalopoulos
function displog(filename)

[program, numOfElectrodes, electrodeName, values, valueName, data] =
parselog(filename);

disp(program)
disp('Electrodes:')
for i = 1:numOfElectrodes,
   disp([' ' num2str(i) '. ' electrodeName{i}])
end
disp('Values:')
for i = 1:values,
   disp([' ' num2str(i) '. ' valueName{i}])
end
```

PLOTLOG SOURCE CODE

```
% PLOTLOG   Plots a Silvaco log file.
% PLOTLOG(filename, x-axis, y-axis, style, xmult, ymult) Creates
% a plot of the value in y-axis vs the value in x-axis with values
% and data derived from filename.log. The line style used is specified
% after that. The x and y values are scaled according to xmult and
% ymult accordingly.

% (c) 2003 by D. C. Gladney----- plotlog function written in 2001 by
% P. Michalopoulos

function plotlog(filename, x, y, p, mx, my)

[program, numOfElectrodes, electrodeName, values, valueName, data] =
parselog(filename);

sx = sign(x);
sy = sign(y);
x = abs(x);
y = abs(y);

if (x > values) | (y > values),
   disp('ERROR! Axis parameter can not be found.')
else
   plot(sx*data(:,x)'*mx, sy*data(:,y)'*my, p), grid on
   title([filename '.log from ' program]);
   xlabel(valueName{x});
   ylabel(valueName{y});
end
```

LIST OF REFERENCES

1. "Space Radiation Environmental Effects," [http://www.eas.asu.edu/~holbert/-eee460/spacerad.html], last accessed 3 June 2004.

2. *ATLAS Users Manual*, SILVACO International, Santa Clara, California, June 1995.

3. T. R. Weatherford, EC3220 Lecture Notes, Naval Postgraduate School, Monterey, California, Fall 2002 (unpublished).

4. P. Michalopoulos, "A Novel Approach for the Development and Optimization of State-of-the-Art Photovoltaic Devices Using Silvaco," Master's Thesis, Naval Postgraduate School, Monterey, California, March 2002.

5. National Aeronautics and Space Administration (NASA), *Solar Cell Array Design Handbook,* Vol. 1, Jet Propulsion Laboratory, Pasadena, California, October 1976.

6. J. Wilson and J. Hawkes, *Optoelectronics: An Introduction*, Prentice-Hall International Inc., Englewood Cliffs, NJ, 1989.

7. M. J. Lavelle, "Modeling the Effects of Radiation-Induced Defects on InGaAs P-I-N Photodiodes," Master's Thesis, Naval Postgraduate School, Monterey, California, December 2002.

8. "Radiation Tolerant and Radiation Hardened Microelectronics," [http://www.-mrcmicroe.com/Radiation_Effects.htm], last accessed 15 July 2003.

9. S. Michael, EC3230 Lecture Notes, Naval Postgraduate School, Winter 2002 (unpublished).

10. "Whatis.com Online," Retrieved June 21, 2003, from [http://whatis.techtarget.-com/whome/0,289825,sid9,00.html].

11. K. Gill, "Radiation Effects on Optoelectronic Components and Systems," CERN CMS Experiment, December 1992.

12. G. C. Messenger and M. S. Ash, *The Effects of Radiation on Electronic Systems,* Van Nostrand Reinhold Company Inc., New York, pp. 168-169, 1986.

13. R. F. Pierret, *Semiconductor Device Fundamentals*, Addison-Wesley Publishing Company, Inc., pp. 195-300, Reading, Massachusetts, 1996.

14. Radiation Hardness Assurance, [http://lhcb-elec.web.cern.ch/lhcbelec/html/-radiation_hardness.htm], last accessed 4 June 2003.

15. R. J. Walters, S. R. Messenger, G. P. Summers, E. A. Burke, S. M. Khanna, D. Estan, L. S. Erhardt, H. Chun Liu, M. Gao, M. Buchanan, A. J. SpringThorpe, A. Houdayer, and C. Carlone , "Correlation of Proton Radiation Damage in InGaAs-GaAs Quantum-Well Light Emitting Diodes," *IEEE Transactions on Nuclear Science*, Vol. 48, No. 6, pp. 1773-1777, December 2001.

16. M. Green, "The Verification of Silvaco as A Solar Cell Simulation Tool and the Design and Optimization of a Four-Junction Solar Cell," Master's Thesis, Naval Postgraduate School, Monterey, California, June 2003.

17. F. Larin, *Radiation Effects In Semiconductor Devices*, John Wiley & Sons, Inc., New York, 1985.

18. J. J. Wiczer, L. R. Dawson, and C. E. Barnes, "Transient Effects of Ionizing Radiation In Photodiodes", *IEEE Transactions on Nuclear Science*, Vol. NS-28 (6), pp. 4397-4402, December 1991.

19. R. J. Walters, G. P. Summers, E. A. Burke, M. A. Xapsos, and S. R. Messenger, "NIEL and Damage Correlations for High-Energy Protons in Gallium Arsenide Devices ," *IEEE Transactions on Nuclear Science*, Vol. 48, No. 6, pp. 2121-2126, December 2001.

20. S. C. Moss, L. F. Halle, and D. C. Marvin "Effects of Electron Beam Irradiation on Transient Photoluminescence Measurements of GaAs and AlGaAs Double Hetrerostructures," *IEEE Transactions on Nuclear Science*, Vol. 42, No. 6, pp. 2058-2065, December 1995.

21. P. Jayavel, J. Arokiaraj, and T. Soga, "Deep Level Transient Spectroscopic Studies of High-Energy Nitrogen-Irradiated Au/n-GaAs Schottky Barrier Diodes," *Semiconductor Science and Technology*, No. 9, pp. 969-973, September 2002.

22. R. J. Walters, S. R. Messenger, G. P. Summers, E. A. Burke, M. A. Xapsos, E. M. Jackson, and B. D. Weaver, "Correlation Non Ionizing Energy Loss (NIEL) for Heavy Ions," *IEEE Transactions on NuclearScience*, Vol. 46, No. 6, pp. 1595-1602, December 1999.

23. D. E. Reeves, "Comparison of Analytic and Numerical Models with Commercially Available Simulation Tools for the Prediction of Semiconductor Freeze-Out and Exhaustion," Master's Thesis, Naval Postgraduate School, Monterey, California, September 2002.

INITIAL DISTRIBUTION LIST

1. Defense Technical Information Center
   Ft. Belvoir, Virginia

2. Dudley Knox Library
   Naval Postgraduate School
   Monterey, California

3. Professor Sherif Michael, Code EC/Mi
   Department of Electrical and Computer Engineering
   Naval Postgraduate School
   Monterey, California

4. Professor Todd Weatherford, Code EC/WT
   Department of Electrical and Computer Engineering
   Naval Postgraduate School
   Monterey, California

5. Chairman, Code EC
   Department of Electrical and Computer Engineering
   Naval Postgraduate School
   Monterey, California